THE IMPROVED QUASISTATIC METHOD FOR CANDU KINETICS

OPTIMUM ITERATION SCHEMES FOR THE IMPROVED QUASISTATIC METHOD

by

S. SCHAFER

PART B: McMASTER (OFF-CAMPUS) PROJECT*

A Project* Report Submitted in Partial Fulfillment
of the Requirements for the Degree of
Master of Engineering

Department of Engineering Physics
McMaster University
Hamilton, Ontario

December, 1978

*One of two project reports. The other one is designated
PART A: ON-CAMPUS PROJECT

MASTER OF ENGINEERING (1978) McMASTER UNIVERSITY
Department of Engineering - Physics Hamilton, Ontario

TITLE: Optimum Iteration Schemes for the

Improved Quasistatic Method

AUTHOR: Steve Schafer, B.Sc. (McGill University)

SUPERVISOR: A. Dastur (AECL)

NUMBER OF PAGES: vi,84

CONTENTS

CONTENTS

ABSTRACT

General theory of nuclear reactor kinetics is discussed, with emphasis on CANDU* reactors. The numerical solution of the group diffusion equations using the IQS+ method is presented. Several important numerical parameters are studied with reference to a one-dimensional slab reactor undergoing a LOCo accident. These parameters are: number of mesh points in the region of solution, frequency of shape calculations, and convergence criteria.

* Canada - Deuterium - Uranium

\+ Improved Quasi-Static

o Loss of Coolant

ACKNOWLEDGEMENT

I wish to express my gratitude to A. Dastur of Atomic Energy of Canada Limited for his constant assistance and encouragement throughout the course of this work. I also wish to thank Dr. B. Rouben (AECL) whose invaluable discussions were significant to my understanding.

Thanks are due to Dr. O.A. Trojan (AECL) and AECL for enabling me to perform my McMaster Off-Campus Project as an AECL summer student.

1. INTRODUCTION

Present day nuclear power systems require sophisticated numerical methods both for their design and for the unprecedented accuracy now demanded for dynamic analysis. It is particularly important to be able to predict the consequences of both planned and unplanned space dependent transients in the reactor core. For this purpose, the Boltzmann Transport Equation applied to neutrons in a chain reacting assembly provides the basic mathematical statement from which the required results are generated.

In Chapter 2, the neutron group diffusion equations are presented, and their evolution from the Boltzmann Transport Equation is discussed. In this regard, emphasis is placed on Fick's Law and energy spectrum collapsing. The Improved Quasi-static method, a procedure for linearizing the group diffusion equations, is described, along with a method to solve the resulting set of inhomogeneous algebraic equations iteratively.

In Chapter 3, the reactor model and transient used in this study are described. The transient consists of a Loss of Coolant (LOC) reactivity perturbation followed by shut-off rod (SOR) insertion in a one-dimensional reactor.

Optimum values of parameters input into the numerical procedure are investigated in Chapter 4. The parameters studied include the number of space mesh points, the frequency of flux shape calculations, and convergence criteria.

2. CANDU NUCLEAR KINETICS

2-1. General Theory of Nuclear Reactor Kinetics

The primary objective of nuclear reactor kinetics is to calculate the behaviour of a neutron population as a function of space, time and energy in assemblies containing materials of known nuclear properties. Phenomena may include radioactive decay, neutron induced fission, neutron scattering, and neutron absorption. In most cases, neutron transport can be treated as the dispersion of a fluid, which greatly simplifies the calculations. The most important physical parameter to calculate is then $N(\vec{r},\vec{\Omega},E,t)$, which is defined by the statement that $N(\vec{r},\vec{\Omega},E,t)\ dVdEd\Omega$ is the number of neutrons which, at time t, are located in an infinitesimal volume dV containing the point $\vec{r}$, have kinetic energy in an infinitesimal energy range dE about E, and are travelling in a direction contained in the infinitesimal cone of direction $d\Omega$ about $\vec{\Omega}$. The integrodifferential equation for $N(\vec{r},\vec{\Omega},E,t)$ is called the Boltzmann Transport Equation. For a derivation of this equation, the reader is referred to

Reference (1). The essential feature of the transport equation is that it equates the net rate of change of neutrons in the phase volume $dVdEd\Omega$ to the rate of production minus the loss of neutrons in that phase volume.

The solution of the Boltzmann Transport Equation for most heterogeneous reactor assemblies is extremely time-consuming and expensive. Hence, numerous approximations have been devised to facilitate both the design of power reactors and studies of various accident conditions. Before we explicitly describe some of these approximations, it is necessary to define certain parameters.

The first parameter of interest is the net current density, $\vec{J}(\vec{r},E,t)$ which is defined so that $\vec{J}(\vec{r},E,t)\cdot\hat{n}dSdE$ is the net number of neutrons in the energy interval [E,E+dE] which pass through a surface dS whose outward normal is $\hat{n}$ in one second at time t. It can be shown that:(1)

$$\vec{J}(\vec{r},E,t) = \int_{\vec{\Omega}} d\Omega\ \vec{\Omega}\ v(E)\ N(\vec{r},\vec{\Omega},E,t) \qquad 2\text{-}1$$

where v(E) is the scalar velocity at energy E.

The second quantity of interest is the scalar flux density, $\phi(\vec{r},E,t)$, defined such that:

$$\phi(\vec{r},E,t) = v(E)\ \int_{\vec{\Omega}} N(\vec{r},\vec{\Omega},E,t)\ d\Omega \qquad 2\text{-}2$$

The flux density is a quantity which facilitates the calculation of reaction rates. For example, the number of type-x interactions per second, F_x, between neutrons in dE and nuclei in dV is given by:

$$F_x(\vec{r},E,t) = \Sigma_x(\vec{r},E,t)\ \phi(\vec{r},E,t)\ dVdE$$

where Σ_x is the macroscopic cross section for a type-x interaction.

With these preliminaries in mind, we can now write down the neutron balance equation, ie, the net rate of increase of neutrons in dVdE is the difference between their rate of appearance and their rate of disappearance:

$$\frac{d}{dt}\left[\frac{1}{v}\ \phi(\vec{r},E,t)\ dVdE\right] =$$

$$\left[\sum_j \chi_p^j(E)\ (1-\beta^j)\ \int_0^\infty \nu^j\Sigma_f^j(\vec{r},E',t)\ \phi(\vec{r},E',t)\ dE'\right] dVdE$$

$$+ \sum_{i=1}^{I} \chi_i(E)\ \lambda_i C_i(\vec{r},t)\ dVdE - \nabla\cdot\vec{J}(\vec{r},E,t)\ dVdE$$

$$- \Sigma_t(\vec{r},E,t)\ \phi(\vec{r},E,t)\ dVdE$$

$$+ \left[\int_0^\infty \Sigma_s(\vec{r},E'\rightarrow E,t)\ \phi(\vec{r},E',t)\ dE'\right] dVdE \qquad 2\text{-}3$$

The first term on the right-hand side is the rate at which prompt neutrons appear in dVdE. The second term is the rate at which delayed neutrons appear in dVdE from I precursor groups. Precursors are fission products which decay by neutron emission

with some half-life. Photoneutrons are also represented as a precursor group. The third term represents the rate at which neutrons leak out of the phase volume dVdE. The fourth term represents the rate at which neutrons are absorbed in dVdE and scattered out of dVdE. The fifth term represents the rate at which neutrons are scattered into dVdE. We now explicitly define the variables used in 2-3.

$\chi_p^j(E)$ - the fraction of total prompt neutrons emitted by isotope j at energy E

ν^j - the number of neutrons released per fission of isotope j

Σ_f^j - the macroscopic fission cross section of isotope j

β^j - the total yield of delayed precursors from isotope j

$\chi_i(E)$ - the fraction of total delayed neutrons emitted by precursor i at energy E

λ_i - the decay constant for the i'th precursor

$C_i(\vec{r},t)$ - the space-time concentration of the i'th neutron precursor

Σ_t - the total macroscopic absorption cross section including the total macroscopic cross section for scattering out of the energy interval [E,E+dE]

$\Sigma_s(\vec{r},E'\rightarrow E,t)$ - the macroscopic cross section for scattering into the energy interval [E,E+dE] from E'

A second equation relates the rate of change of the i'th neutron precursor to its production and destruction, ie:

$$\frac{\partial C_i(r,t)}{\partial t} = \sum_j \beta_i^j \int_0^\infty \nu^j \Sigma_f^j(\vec{r},E',t)\ \phi(\vec{r},E',t)\ dE'$$

$$- \lambda_i C_i(\vec{r},t),\ i = 1, 2, \ldots, I \qquad 2\text{-}4$$

where β_j^i is the fraction of the precursor i produced per fission of isotope j. There are I groups of precursors. Note that:

$$\beta^j = \sum_{i=1}^{I} \beta_i^j \qquad 2\text{-}5$$

Equations 2-3 and 2-4 represent the fundamental mathematical statements of nuclear reactor kinetics. We note, however, that there are 2 + I unknown functions, ϕ, $\vec{J}$ and C_i, i = 1, ..., I, and only 1 + I equations. Hence, another equation is needed to relate $\vec{J}$ and ϕ. This equation is known as Fick's Law, and states that the neutron current density is directly proportional to the gradient of the flux density, ie:

$$\vec{J}(\vec{r},E) = -D(\vec{r},E)\ \nabla\phi(\vec{r},E) \qquad 2\text{-}6$$

where $D(\vec{r},E)$ is called the diffusion constant. For a derivation of Fick's Law directly from the Boltzmann Transport Equation, the reader is referred to Reference (1). While we shall not prove Equation 2-6, we shall discuss its plausibility and its limitations, since Fick's Law currently represents one of the most important approximations utilized in reactor physics calculations.

Equation 2-6 states that for neutrons at energy E, the net current across a surface is proportional to the rate of decrease of the density of neutrons across that surface. Moreover, the direction of the net current is the direction in which the number of neutrons is decreasing at its maximum rate. Thus, the neutron population tends to drift from a region of high concentration to one of low concentration, like a gas diffusing through a porous plug, and this drift gives rise to a net current. Equation 2-6 represents the starting point for neutron diffusion theory.

One method of obtaining Equation 2-6 is to assume that $N(\vec{r},\vec{\Omega},E,t)$ has the form:

$$N(\vec{r},\vec{\Omega},E,t) = [\phi(\vec{r},E,t) + \frac{3}{4\pi}\vec{\Omega}.\vec{J}(\vec{r},E,t)]\ v(E) \qquad 2\text{-}7$$

It can easily be shown that Equations 2-1 and 2-2 are consistent with this form of $N(\vec{r},\vec{\Omega},E,t)$. The neutron distribution described by Equation 2-7 is said to be linearly anisotropic. It is clear that Equation 2-7 cannot describe neutron population distributions which are strongly anisotropic. Hence, Fick's Law will not be valid near the outside surface of a reactor and near or within strong absorbers, where strong anisotropy will exist due to rapid variations in scattering and absorption cross sections.

Equations 2-3, 2-4 and 2-6 represent, in principle, the equations of neutron diffusion theory. However, their energy dependence makes them difficult to solve, so further approximations resulting in the energy-group diffusion equations are used. The essential approximation is that the flux density, $\phi(\vec{r},E,t)$, in the energy group $\Delta E_g = [E_g, E_{g-1}]$, may be written:

$$\phi(\vec{r},E,t) = \phi_g(\vec{r},t)\ \psi_g(\vec{r},E) \qquad 2\text{-}8$$

where we assume that $\psi_g(\vec{r},E)$ can be determined for different regions from the nuclear data and isotopic concentrations of materials throughout the reactor. $\psi_g(\vec{r},E)$ is defined so that:

$$\int_{E_g}^{E_{g-1}} \psi_g(\vec{r},E)\ dE = 1.0 \qquad 2\text{-}9$$

Using 2-6, 2-8 and 2-9 in 2-3, we obtain for G groups:

$$\frac{1}{v_g(\vec{r})}\frac{d}{dt}\phi_g(\vec{r},t) = \sum_{g'}\left[\sum_j \chi^j_{pg}(1-\beta^j)\ \nu^j\ \Sigma^i_{fg'}(\vec{r},t)\ \phi_{g'}(\vec{r},t)\right]$$

$$+ \sum_i \chi_{ig}\ \lambda_i C_i(\vec{r},t) + \nabla.D_g(\vec{r},t)\ \nabla\phi_g(\vec{r},t)$$

$$- \Sigma_{tg}(\vec{r},t)\ \phi_g(\vec{r},t) + \sum_{g'}\left[\Sigma_{g',g}(\vec{r},t)\ \phi_{g'}(\vec{r},t)\right] \qquad 2\text{-}10$$

$$g' = 1, 2, \ldots, G$$

where:

$$\frac{1}{v_g(\vec{r})} = \int_{\Delta E_g} \frac{1}{v(E)} \psi_g(\vec{r},E)\, dE$$

$$\phi_g(\vec{r},t) = \int_{\Delta E_g} \phi(\vec{r},E,t)\, dE$$

$$\chi^j_{pg} = \int_{\Delta E_g} \chi^j_p(E)\, dE$$

$$\Sigma^j_{pg'} = \int_{\Delta E_{g'}} \Sigma^j_f(\vec{r},E',t)\, \psi_{g'}(\vec{r},E')\, dE'$$

$$\chi_{ig} = \int_{\Delta E_g} \chi_i(E)\, dE$$

$$D_g(\vec{r},t) = \int_{\Delta E_g} D(\vec{r},E,t)\, \psi_g(\vec{r},E)\, dE$$

$$\Sigma_{tg}(\vec{r},t) = \int_{\Delta E_g} \Sigma_t(\vec{r},E,t)\, \psi_g(\vec{r},E)\, dE$$

$$\Sigma_{g'g}(\vec{r},t) = \int_{\Delta E_g} dE \int_{\Delta E_{g'}} \Sigma_s(\vec{r},E' \to E)\, \psi_{g'}(\vec{r},E')\, dE'$$

Equation 2-4 reduces to:

$$\frac{\partial C_i(\vec{r},t)}{\partial t} = \sum_{g'} \left[\sum_j \beta^j_i\, \nu^j\, \Sigma^j_{fg'}(\vec{r},t)\, \phi_{g'}(\vec{r},t)\right]$$

$$-\lambda_i C_i(\vec{r},t) \qquad 2\text{-}11$$

Equations 2-10 and 2-11 represent multi-group diffusion theory. We can see that the problem of solving for group fluxes can be made simplest by using as few groups as necessary in the analysis, while sacrificing some accuracy.

2-2. Some Specifics of CANDU Kinetics

The CANDU PHW nuclear power system is a heavy water moderated pressure tube type reactor. Figure 1 displays a typical reactor assembly. There are several neutron kinetic peculiarities associated with this type of reactor design. Firstly, for short (several seconds) transients, it is adequate to perform most calculations using six delayed neutron groups.[2] Secondly, the reactor is so well moderated that two energy groups are sufficient.[3] Thus, Equations 2-10 and 2-11 reduce to:

GROUP 1 (fast)

$$\frac{1}{v_1}\frac{d}{dt}\phi_1(\vec{r},t) = (1-\beta)\,\nu\Sigma_f\,\phi_2(\vec{r},t), + \sum_{i=1}^{6}\lambda_i C_i(\vec{r},t)$$

$$+ \nabla.D_1(\vec{r},t)\,\nabla\phi_1(\vec{r},t) - \Sigma_{t1}(\vec{r},t)\,\phi_1(\vec{r},t) \qquad 2\text{-}12$$

GROUP 2 (slow)

$$\frac{1}{v_2}\frac{d}{dt}\phi_2(\vec{r},t) = \nabla.D_2(\vec{r},t)\,\nabla\phi_2(\vec{r},t)$$

$$- \Sigma_{t2}\,\phi_2(\vec{r},t) + \Sigma_{12}\,\phi_1(\vec{r},t) \qquad 2\text{-}13$$

DELAYED NEUTRON PRECURSORS

$$\frac{\partial C_i}{\partial t} = \beta_i\,\nu\Sigma_f\,\phi_2(\vec{r},t) - \lambda_i C_i(\vec{r},t) \qquad 2\text{-}14$$

$$i = 1, \ldots, 6$$

Note that in the above notation we have omitted reference to the superscript j, and hence we are limiting the calculation to one fissionable isotope (unless the group cross sections are updated to account for fuel burnup). It should be noted that for long-term transient and fuel burnup studies, it may be necessary to include up to 33 delayed neutron precursor groups.

Other physics and engineering factors which affect space dependent neutron transients in CANDU reactors have been studied by Dastur and Buss.[4] Major factors were found to be:

1. Neutronic decoupling of reactor segments due to deliberate flattening of the power distribution.
2. Retardation of the power shape transient due to delayed neutron holdback.
3. Photoneutron production in heavy water.
4. Asymmetric insertion of reactivity devices.

2-3. Numerical Solution of the Group Diffusion Equations

There are numerous spatial approximation and time integration methods available for the solution of the space-time dependent neutron group diffusion equations. For example, one can employ techniques of Finite Difference, Modal Expansion, Nodal Expansion, and Factorization. A review of the principles behind each of these methods can be found in Reference (5). For this work, the Improved Quasi-Static (IQS) method has been used. We first describe the factoring procedure and obtain the point kinetics equations. We next describe how the flux distribution is generated using the IQS method.

2-3-1. The Point Kinetics Equations

It is necessary to introduce the fast and slow time independent (static) adjoint fluxes, defined by the equations:

$$\begin{aligned} \nabla . D_1(\vec{r})\ \nabla\psi_1^*(\vec{r}) - \Sigma_{t1}\ \psi_1^*(\vec{r}) + \Sigma_{12}\ \psi_2^*(\vec{r}) &= 0 \\ \nabla . D_2(\vec{r})\ \nabla\psi_2^*(\vec{r}) - \Sigma_{t2}\ \psi_2^*(\vec{r}) + \nu\Sigma_f\ \psi_1^*(\vec{r}) &= 0 \end{aligned} \qquad 2\text{-}15$$

The use of the adjoints shall soon become apparent. The physical meaning of the adjoint function is as follows: Assume we introduce K neutrons, all with energies in one group, into a small volume dV of a critical reactor. If the initial neutron population is N_o, and the asymptotic neutron population is $N_o+\Delta N$, then it can be shown that:[1]

$$\psi_g^*(\vec{r}) \propto \frac{\Delta N}{K} \qquad 2\text{-}16$$

$\psi_g^*(\vec{r})$ is called the "neutron importance" at the point $\vec{r}$, and represents the increase in asymptotic population level caused by one neutron introduced at $\vec{r}$ in group g. We note that the above description of neutron importance is simplified, since ψ_g^* will be sensitive to both the energy and direction of a neutron in the core, as well as its position. For example, a large fraction of fast neutrons introduced into the reflector of a reactor would escape without causing any increase in neutron population level, and hence this region is considered to have small importance when neutrons are travelling away from the core. For a more complete

discussion of neutron importance, the reader is referred to Reference (1).

We now introduce a quantity AMP(t), the amplitude function, defined by:

$$AMP(t) = \int_{REACTOR} dV \left[\psi_1^*(\vec{r}) \frac{\phi_1(\vec{r},t)}{v_1} + \psi_2^*(\vec{r}) \frac{\phi_2(\vec{r},t)}{v_2}\right] \qquad 2\text{-}17$$

AMP(t) is clearly the integral of the fast and slow neutron densities, each weighted by its respective importance. For a point reactor, AMP(t) is directly proportional to the power. Additionally, we require that AMP(0) = 1, as can be accomplished by multiplying the adjoints by a suitable constant.

Next, we introduce a group shape function $\psi_g(\vec{r},t)$, defined such that:

$$\phi_g(\vec{r},t) = AMP(t) * \psi_g(\vec{r},t) \qquad 2\text{-}18$$

Substituting 2-18 into 2-17, we find that:

$$\int_{REACTOR} dV \left[\psi_1^*(\vec{r}) \frac{\psi_1(\vec{r},t)}{v_1} + \psi_2^*(\vec{r}) \frac{\psi_2(\vec{r},t)}{v_2}\right] = 1 \qquad 2\text{-}19$$

If we substitute Equation 2-18 into Equations 2-12, 2-13 and 2-14, and then integrate Equation 2-14, we obtain:

$$\frac{1}{v_1} \frac{\partial \psi_1(\vec{r},t)}{\partial t} = (\nabla . D_1(\vec{r},t) \nabla - \Sigma_{t1} - \frac{\dot{AMP}(t)}{v_1 \, AMP(t)}) \psi_1(\vec{r},t)$$

$$+ (1 - \beta) \nu\Sigma_f \psi_2(\vec{r},t) + \frac{1}{AMP(t)} \sum_{i=1}^{6} \lambda_i C_i(\vec{r},t) \qquad 2\text{-}20$$

$$\frac{1}{v_2}\frac{\partial \psi_2(\vec{r},t)}{\partial t} = (\nabla . D_2(\vec{r},t)\ \nabla - \Sigma_{a2} - \frac{\dot{AMP}(t)}{v_2 AMP(t)})\ \psi_2(\vec{r},t)$$

$$+ \Sigma_{12}\ \psi_1(\vec{r},t) \qquad 2\text{-}21$$

$$C_i(\vec{r},t) = C_i(\vec{r},0)\ e^{-\lambda_i t}$$

$$+ \int_0^t \beta_i\ \nu\Sigma_f\ \psi_2(\vec{r},t')AMP(t')\ e^{-\lambda_i(t-t')}\ dt' \qquad 2\text{-}22$$

In the above equations, $\dot{AMP}(t)$ is the rate of change of the amplitude function with respect to time. Next we multiply Equation 2-20 by $\psi_1^*(\vec{r})$ and Equation 2-21 by $\psi_2^*(\vec{r})$, integrate both equations over the whole reactor volume, and add the two resulting equations together. The result is:

$$\dot{AMP}(t) = (\frac{\rho(t) - \beta}{\Lambda(t)})\ AMP(t) + \sum_{i=1}^{6} \lambda_i\ n_i(t) \qquad 2\text{-}23(a)$$

where (using $< f, g > = \int_{REACTOR} fg\ dV$)

$$\rho(t) = \Lambda(t)\ [<\psi_1^*(\vec{r}),\ [\nabla . D_1 \nabla\ - \Sigma_{t1}]\ \psi_1(\vec{r},t) + \nu\Sigma_f\ \psi_2(\vec{r},t)>$$

$$+ <\psi_2^*(\vec{r}),\ [\nabla . D_2 \nabla - \Sigma_{a2}]\ \psi_2(\vec{r},t) + \Sigma_{12}\ \psi_1(\vec{r},t)>]$$

$$\Lambda(t) = \frac{1}{<\psi_1^*(\vec{r}),\ \nu\Sigma_f\ \psi_2(\vec{r},t)>} \qquad 2\text{-}23(b)$$

$$n_i(t) = <\psi_1^*(\vec{r}),\ C_i(\vec{r},t)>$$

$$\beta = \sum_{i=1}^{6} \beta_i$$

If Equation 2-18 is used in 2-14, and the result multiplied by $\psi_1^*(\vec{r})$ and integrated over the reactor volume, we obtain:

$$\dot{n}_i = \frac{\beta_i}{\Lambda(t)} AMP(t) - \lambda_i n_i \qquad 2\text{-}24$$

Equations 2-23(a) and 2-24 are called the point kinetics equations, and for many years have formed the basis of almost all transient design analysis performed for reactors. Their exclusive use depends to a large extent on the fact that for many transients of practical interest, the flux shapes change very little, hence the kinetics parameters, (ρ, Λ, n_i) can be calculated using the initial flux shape throughout the entire transient. This procedure leads to excellent results for the amplitude function, which is a measure of the time variation of the total neutron population, if the reactor is relatively small and its segments are well coupled, as with early research reactors. Modern day power reactors require more sophisticated methods due to their large size and the accuracy demanded for complex accident analysis.

2-3-2. The Meaning of the Kinetics Parameters

The parameter $\rho(t)$ is called the reactivity of the reactor. Careful inspection of the numerator of the equation for $\rho(t)$ shows that it is an integral of the net instantaneous production of neutrons in the reactor, weighted by the importance

function. The denominator is the instantaneous production rate due to fission, weighted by the importance function. Reactivity is, then, the ratio of this net weighted rate to the weighted production rate due to fission. It can be thought of as the fractional increase of importance per generation due to fission neutrons.

The quantity $\Lambda(t)$ is called the prompt-neutron generation time. The equation for can be rewritten as follows:

$$\Lambda(t) = \frac{AMP(t)}{\langle \psi_1^*(\vec{r}),\ \nu\Sigma_f\ \phi_2(\vec{r},t) \rangle}$$

The numerator of the right-hand side is equal to the total number of fast and slow neutrons in the reactor, weighted by the respective importance. The denominator is the weighted production rate of all neutrons. Hence, Λ can be interpreted as the time a neutron of average importance survives after it appears either as a prompt neutron or one emitted from a delayed neutron precursor.

It should be noted that these interpretations of ρ and Λ depend on the importance remaining approximately the same throughout the transient. In cases where regions greatly change their material properties during the transients (such as a fast shutdown), the physical interpretation of the kinetics parameters is elusive. Use of time-dependent importance functions would aid interpretation but would immensely complicate and add significant cost to numerical procedures.

2-3-3. The IQS Methods

Equations 2-20, 2-21 and 2-22 are solved by the Improved Quasistatic Approximation (IQS).[6] The important difference between the IQS method and other quasistatic methods is that it replaces the derivative of $\psi_g(\vec{r},t)$ by a backward difference of first order:

$$\frac{\partial}{\partial t}\psi_g(\vec{r},t) = \frac{\psi_g(\vec{r},t) - \psi_g(\vec{r},t-\Delta t)}{\Delta t} \qquad 2\text{-}25$$

where $t - \Delta t$ is the time of the last shape calculation. It can be shown (see, for example, Reference (5)) that the backward difference approach is numerically stable for large time steps, but that the forward difference approach is not. In the next sections, we describe the numerical procedures used to solve the shape, neutron precursor, and point kinetics equations to obtain a complete space-time representation of the neutron flux.

2-3-4. The Numerical Procedure

The shape, precursor, and point kinetics equations are coupled. Hence, in order to obtain accurate numerical solutions, it is necessary to iterate several times between the equations in order to perform the current calculations with updated values from the previous calculation. We now list the stages of calculation used in this study:

1. The static (exactly critical) model is set up.
2. Equations 2-20 and 2-21 are solved with:

   (a) $\frac{\partial \psi_g}{\partial t}(\vec{r}, t=0) = 0$

   (b) $\dot{AMP}(0) = 0$

   (c) $C_i(\vec{r}, 0) = \frac{\beta_i \nu\Sigma_f \phi_2(\vec{r}, 0)}{\lambda_i}$

   This step gives the static flux shape and the initial precursor concentration.
3. Equations 2-15 are solved, to give the static adjoint fluxes. The adjoints are adjusted so that Equation 2-19 is satisfied at t = 0.
4. The reactor model is changed in accordance with the transient conditions at a particular time, t_{NEW}, into the transient.
5. Equations 2-20 and 2-21 are solved using the amplitude and the time derivative of the amplitude from the previous time, t_{OLD}. In Equation 2-20, $C_i(\vec{r}, t)$ is given by Equation 2-22 with:

$$\psi_2(\vec{r}, t) = \psi_2(\vec{r}, t_{OLD}) + \left(\frac{\psi_2(\vec{r}, t_{NEW}) - \psi_2(\vec{r}, t_{OLD})}{t_{NEW} - t_{OLD}}\right)(t - t_{OLD}) \qquad 2\text{-}26$$

6. New values for $\rho(t)$ and $\Lambda(t)$ are calculated using the new shape functions from step 5.

7. The time interval ($t_{NEW} - t_{OLD}$) is broken up into smaller time intervals, ρ is linearly interpolated over this time interval, and the point kinetics equations are solved.
8. Equations 2-20 and 2-21 are re-solved using the updated $AMP(t_{NEW})$ and $\dot{AMP}(t_{NEW})$.
9. Using the results of step 8, the kinetic parameters are updated.
10. The precursor concentrations are updated using Equation 2-22.
11. Steps 4 to 10 are repeated for a new time.

For convenience, steps 5 to 6 shall be known as the "A" case, step 7 as the amplitude calculation, and steps 8 to 10 as the "B" case. Several features of the above procedure should be pointed out:

1. It is unlikely that an exactly critical reactor will be set up the first try. When Equations 2-20 and 2-21 are solved for the static flux shape, a number, EOK, is determined such that when $\nu\Sigma_f$ is replaced by $\nu\Sigma_f/EOK$, the reactor is exactly critical. All subsequent $\nu\Sigma_f$'s must be corrected by EOK.
2. When the reactivity, $\rho(t)$, is interpolated in step 7 (the amplitude calculation), the value of $\rho(t_{NEW})$ is taken from the "A" case which has just

been completed. The value of $\rho(t_{OLD})$ is taken from the previous "A" case, and not from the previous "B" case.

3. The shape function varies considerably slower than the amplitude function. This is the reason for using relatively large time intervals between shape calculations (performed in the "A" and "B" cases), and breaking this time interval up in step 7 (the amplitude calculation).

2-3-5. The Numerical Solution of the Shape Equations

Equations 2-20 and 2-21 represent the equations to be solved to obtain the flux shape. We have described in section 2-3-3 the way in which the IQS method deals with the time derivative term. We now show how the space derivative term is calculated.

The reactor is first broken up into small cells, of dimensions ΔX, ΔY and ΔZ. In a typical CANDU cell, ΔX and ΔY correspond to one lattice pitch and ΔZ to one fuel bundle length. Equations 2-20 and 2-21 are then integrated over the cell volume. The space derivative term, which represents the leakage from the cell now becomes:

$$\text{LEAKAGE} = \int_{cell} \nabla . D_g(\vec{r},t) \nabla \psi_g(\vec{r},t) \, dV$$

or, using the divergence theorem:

$$\text{LEAKAGE} = \int_{\substack{\text{surface}\\ \text{of cell}}} D_g(\vec{r},t)\ \nabla\ \psi_g(\vec{r},t)\ .\ \vec{dA} \qquad 2\text{-}27$$

where $\vec{dA}$ is a vector elemental area which is outward normal to the cell surface. Figure 2 shows three representative cells. We now show how the leakage is calculated through the shaded area in Figure 2 between the (I - 1)'th and I'th cells. The flux must be continuous at the boundary, so let ψ_g be the value of the shape function at the boundary. The neutron current must be continuous at the boundary, hence:

$$D_g \frac{\partial \psi_g}{\partial X}_{\text{boundary}} = D_g(I-1)\frac{[\psi_g - \psi_g(I-1)]}{\Delta X(I-1)*\frac{1}{2}}$$

$$= D_g(I)\ \frac{[\psi_g(I) - \psi_g]}{\Delta X(I)*\frac{1}{2}} \qquad 2\text{-}28$$

$$\Longrightarrow \qquad \psi_g = \frac{\Delta X(I-1)\ D_g(I)\ \psi_g(I) + \Delta X(I)\ D_g(I-1)\ \psi_g(I-1)}{D_g(I)\ \Delta X(I-1) + D_g(I-1)\ \Delta X(I)} \qquad 2\text{-}29$$

Using 2-27, 2-28 and 2-29, we find:

LEAKAGE THROUGH SHADED AREA IN FIGURE 2 =

$$\frac{2\ D_g(I)\ D_g(I-1)\ [\psi_g(I) - \psi_g(I-1)]\ \Delta Y\ \Delta Z}{D_g(I)\ \Delta X(I-1) + D_g(I-1)\ \Delta X(I)} \qquad 2\text{-}30$$

In order to calculate the leakage from all sides of the cell, equations analogous to 2-30 are used for each cell face. This procedure yields 2N linear difference equations with the fast and

thermal shape functions as unknown variables at N points in the reactor. This set of algebraic equations may be presented as a matrix equation:

$$A\bar{\psi} = \bar{Y} \qquad 2\text{-}31$$

While this equation may be solved by Gaussian elimination, it is considerably cheaper to solve it iteratively. The method used is called the Gauss-Seidel method with provisions made for the employment of Liebmann over-relaxation. This procedure is described more fully in Appendix 1.

2-3-6. Conditions for Convergence

The basic assumption in the IQS method is that both the time rate of change of the spatial flux, $\psi_g(\vec{r},t)$, and the time rate of change of reactivity, $\rho(t)$, are linear over a time interval. These conditions can be satisfied if the time interval is chosen small enough so that further reductions in its size do not lead to improvements in the desired accuracy.

As described in section 2-3-5, the above assumptions lead to a set of algebraic equations which are solved by the Gauss-Seidel iteration method. There are three major conditions in the numerical procedure which must be satisfied if the method is to yield the correct solution to the diffusion equations. These conditions presuppose that the assumptions outlined in the previous paragraph are reasonably satisfied.

The first condition is that Equation 2-19 must be satisfied at the end of each shape calculation.

The linearization of Equations 2-20 and 2-21 yields 2N equations in 2N unknowns, where N is the number of mesh points. Hence, Equation 2-19 represents the (2N+1)'th equation, an overspecification to the set of linear algebraic equations to be solved. (The entire problem is not overspecified.) It is found that the Gauss-Seidel method with Liebmann over-relaxation by itself leads to slow convergence. Hence, to speed convergence, an empirical method was developed to include an extra degree of freedom in the calculation. This method requires that every term containing $\nu\Sigma_f$ in the set of algebraic equations is divided by a number, KE_n, such that:

$$KE_n = \frac{SUMM_n}{SUMM_{n-1}} * KE_{n-1} \qquad 2\text{-}33$$

where n refers to the n'th iteration, and:

$$SUMM_n = \sum_{(I,J,K)} [\psi_1^n(I,J,K) + \psi_2^n(I,J,K)] \qquad 2\text{-}34$$

The second condition to be satisfied is, then:

$$KE_{n_f} = EOK \qquad 2\text{-}35$$

where n_f is the number of the final iteration, and EOK was defined in section 2.

The third condition to be satisfied is:

$$\text{EPS} \geq \left| \frac{\psi_1^n(I,J,K) + \psi_2^n(I,J,K)}{\psi_1^{n-1}(I,J,K) + \psi_2^{n-1}(I,J,K)} - 1 \right| \qquad 2\text{-}35$$

where EPS is an input parameter. Equation 2-35 must be satisfied for every point (I,J,K) in the reactor before the calculation terminates. An important point to note is that if the iteration is converging very slowly, Equation 2-35 may be satisfied even though the current values for the ψ_g's may be far from the solution of the algebraic equations. Hence, EPS is not a parameter which gives the absolute error between the calculated solution and the exact solution, but merely provides a convenient method for exiting from the iteration loop when it becomes likely that sufficient accuracy has been reached.

3. DESCRIPTION OF STUDY

3-1. The Reactor Model

The model was chosen to satisfy several requirements. Firstly, it was necessary to keep the calculations cheap, so a one-dimensional model was used for the study, as shown in Figure 3. The reactor is 600 cm in length, and consists of four basic regions whose properties are listed in Table 1. The mesh spacing was non-uniform. The boundary condition used was that the flux goes to zero at .7104 λ_{tr} from the surface of the reactor.

The production cross sections ($\nu\Sigma_f$) for the different regions were chosen to emphasize neutronic decoupling. This is illustrated by the dished flux distribution shown in Figure 4.

3-2. The Transient

The transient was chosen to satisfy several requirements:

1. Delayed neutron holdback was emphasized. Table 2 displays the delayed neutron data used for this work, taken from Reference (2).

2. The transient was representative of those encountered in safety analysis. To satisfy this requirement, a loss of coolant (LOC) type reactivity perturbation was assumed. Figure 5 shows the reactivity perturbation as a function of time. The reactivity insertion due to LOC is included in the transient by changing $\nu\Sigma_f$ in the following manner:

$$\nu\Sigma_f(x,t) = \nu\Sigma_f(x,0)\ [1 + \rho'(t)] \qquad 3\text{-}1$$

where $\rho'(t)$ is taken from Figure 5.

3. The transient was sub-prompt critical in order to represent a typical CANDU transient.
4. There was a large change in the flux shape during the transient. This was accomplished by perturbing the right half of the reactor with the LOC type reactivity perturbation, and having the shut-off rod (SOR) moving into the left half. Table 3 displays the SOR incremental properties. Figure 6 shows the rate at which the SOR moves into the reactor. The rod is 540 cm in length, and sits symmetrically in the reactor at the end of the transient. Hence, the rod is considered to be 100%

inserted in the 600 cm reactor when it has travelled 570 cm into the reactor from the left. A 0.4 second delay was assumed between the beginning of the LOC and the triggering of the SOR.

3-3. Parameters Studied

The effects of changing the following parameters were studied:

1. Frequency of the shape calculation.
2. Number of mesh points.
3. The convergence parameter, EPS, where EPS is the number which determines when the iteration terminates, as described in section 2-3-6.

The frequency of shape calculations is determined by the time step between A (or B) cases. Tables 4 to 7 display the input data for the time steps studied. Rather than referring to a time step in seconds, we shall refer to the distance travelled by a SOR, which directly determines the time step from Figure 6. The time steps studied correspond to rod movements of 20, 10, 5 and 2.5 centimeters per time step.

The study of the number of mesh points used 20 cm time steps. Two cases were studied; 60 mesh points and 34 mesh points. Larger mesh spacings were not investigated, since this would require smearing of SOR properties, which introduces

another independent variable into the study and complicates the analysis. Table 8 shows the geometry used for the 34 mesh point case. For the 60 mesh point case, the position, P(I), of the I'th mesh point is given by:

$$P(I) = (10I - 5) \text{ cm}$$

The study of EPS used the best converged time step. Hence, cases 3 to 96 used 10 cm time steps, cases 97 to 108 used 5 cm time steps, and cases 109 to 244 used 2.5 cm time steps. EPS = 10^{-6}, 10^{-5}, 10^{-4}, and 10^{-3} were studied.

The value of KE was kept constant for the first five iterations of every case. The Liebmann acceleration parameter was set equal to 1.5.

4. RESULTS

4-1. Variation of Time Step

The time steps studied corresponded to 20, 10, 5 and 2.5 cm rod movements per time step. The mesh spacing used was 10 cm, so there were 60 mesh points. EPS = 10^{-6} was the convergence criterion, and in all cases Equation 2-19 was satisfied.

Since the mesh points were 10 cm apart, it was necessary to smear SOR properties over the cell for 5 and 2.5 cm time steps. For example, if the SOR was 7.5 cm into the 10 cm cell, the SOR properties input for that cell were .75 times the values for full insertion. In comparing the results of different runs, it is important to keep this fact in mind, since the smearing will cause the flux in the cell (and adjacent cells) to drop faster. This is because in cases where there is no smearing, the cell must await the full time step for complete insertion of the SOR. The cases of no smearing would seem to be the most conservative from a safety point of view, but may in fact be incorrect due to the length of the time step, violating the linearity assumptions described in section 2-3-6.

Figure 7 shows (KE_{n_f}/EOK -1) versus time for different runs. Firstly, it can be seen that deviation from zero begins at ~ 1.8 seconds into the transient. At this time, the rod is 430 cm into the reactor. It can be seen from Figure 4 that the rod is beginning to enter the high flux region, hence the shape of the flux is expected to change with time more quickly than before and smaller time steps are needed. Figure 7 also shows that halving the time step approximately halves the maximum deviation of (KE_{n_f}/EOK -1) from zero. The strange behaviour of the 5 cm time step curve after 2.0 seconds has not been satisfactorily explained.

Table 9 shows the $\int_{\text{REACTOR}} \nu\Sigma_f \, \phi_2(X,t) \, dV$ versus time for the various time steps. It can be seen that the differences between the runs is less than 1% for all times.

Table 10 shows the relative maximum of the flux shape and its position. It can be seen that the position of the maximum flux is identical in all cases. The difference between shape values for the two cases with smearing is < 1% for each time. The difference between the two nonsmearing cases is < 3% for all times. The difference between the 10 cm time step (no smearing) case and 5 cm time step (smearing) case is < 2% for all times. The maximum difference between any two tabulated values at the same time is ~ 6%.

Table 11 shows the relative values of the thermal flux shape function for two positions in the reactor versus time for

the different time steps. At 495 cm, the maximum difference between any value at the same time is ~ 3%. There is less than 1.0% gain in going from 20 cm time steps to 10 cm time steps. There is less than 1.5% gain in going from 5 cm time steps to 2.5 cm time steps. At 105 cm, there is a maximum of ~ 8% difference between cases with no smearing, and a maximum of ~ 3% difference for the cases with smearing. However, between any value at the same time, the error is as much as 20% (see T = 1.97 sec in Table 11).

Table 12 shows the value of the total leakage divided by the total production. It can be seen that the percent differences between values become greatest at about the same times as when KE_{nf} does not converge to EOK. This is reasonable, since the leakage depends on the flux gradients, which are rapidly changing during this time.

Since the calculation of the total energy generation during a transient will be strongly dependent on the amplitude function, this parameter is probably the most important to examine. Tables 13 and 14 display the reactivity and amplitude functions at various times during the transient.

The first feature of interest is the rather large value of the dynamic reactivity at the end of the transient. In the one-dimensional model used, the SOR is considered to be a large slab moving uniformly into the reactor from one side. Since the SOR properties used were representative of a CANDU reactor, the

final dynamic reactivity turns out to be unrealistic. This does not effect tie results of this study, since the flux gradients produced are realistic, and the information obtained from the analysis of the results is applicable to realistic cases.

A second feature of interest is that the amplitude function and reactivity decrease faster for the cases where there is smearing. This phenomenon has already been explained at the beginning of this section. It is expected that this effect shall not be nearly as large in a real study, since smearing effects will be localized.

From Table 14, it can be seen that there are differences of up to 10% between the two cases where there is no smearing. The maximum errors exist at the same time as when the reactivities and KE_{n_f} disagree the most. This information indicates that too large a time step has been chosen. This prevents KE_{n_f} from converging to EOK, resulting in incorrect reactivities. When these reactivities are fed into the point kinetics equations, the resulting amplitudes are erroneous.

Since the 5 and 2.5 cm time step studies involved smearing, they cannot be compared to the 20 cm and 10 cm time step studies consistently. It is suggested, therefore, that this study must be pursued with smaller mesh spacings, perhaps of 2.5 cm. Furthermore, the effects of smearing should be examined in greater detail with parallel studies. It is interesting to note that Garvey[7] has concluded that there is no a-priori method of determining the required length of the time steps apart from the experience gained by the analysis of similar cases.

4-2. Number of Mesh Points

This study examined the effects of using 34 and 60 mesh points. Smearing of the SOR properties was avoided by choosing 20 cm time steps and a minimum of 34 mesh points. This has the disadvantage that such large time intervals did not allow convergence, as illustrated by Figure 8, which also shows that the values of $(KE_{n_f}/EOK - 1)$ versus time are approximately equal for the two cases, even when nonconverged. This difficulty will not affect the results, since if the transients are identical except for number of mesh points, a comparison is valid. Another disadvantage is that smaller numbers of mesh points could not effectively be studied without significant smearing of SOR properties.

A comparison of $\int \nu\Sigma_f \, \phi_2(t) \, dV / \int \nu\Sigma_f \, \phi_2(0) \, dV$ at different times is shown in Table 15. It can be seen that the difference between the two cases is < .2% for all times. Table 16 shows the FORM FACTOR, where:

$$\text{FORM FACTOR} = \frac{\int \nu\Sigma_f \, \phi_2 \, dV}{(\int \nu\Sigma_f \, dV) \, \phi_2^{max}}$$

The differences observed in Table 16 may be due to the fact that the ϕ_2^{max} were not taken at exactly the same point for each model because of the geometry chosen. This is illustrated in Table 17, which compares the maximum shape function at different times to its initial value. It can be seen that the positions of the maxima are never more than 5 cm apart in the two models. This is the minimum difference allowed due to the models chosen.

Tables 18 and 19 display the reactivity and amplitude functions. Two questions are suggested by the data:

1. What causes the sudden large differences at t = 1.68 seconds and 1.77 seconds?
2. After the results have diverged so extensively, how do they manage to return to similar magnitudes at later times?

Figures 9 to 12 display the flux shapes at various times during the transient. It can be seen that there is a negligible difference between the two models. Since the integral quantities used to calculate the amplitude depend on the flux shapes, it would be expected that only small differences between the amplitudes calculated from the two models would be obtained. However, the integrals have been calculated by multiplying the cell value of the shape function by the cell volume by the appropriate cross section. This method assumes that the flux behaves as a step-like function from cell to cell. This assumption may be the cause of the large differences between the two models for certain flux shapes. For example, the large flux tilts at T = 1.68, 1.77, and 2.01 seconds, may cause the assumption to break down due to the large flux gradients. This suggests that a flux interpolation method may yield adequate results with fewer mesh points.

Ott and Meneley[8] have pointed out that the calculation of the flux shape is relatively insensitive to errors in the amplitude and its time derivative for cases of practical

interest. Hence, if the delayed neutron precursor population is correctly calculated after each time step, then the flux shape will depend almost entirely on the current reactor material configuration. There is a reason for the delayed neutron source distribution to be correct even though the current flux shape may be in error. This is because there is negligible precursor production during the transient and the pre-event precursor distribution dominates during the transient. Therefore, the delayed source distribution is quite independent of the current reactor configuration. Since the accuracy of the integral parameters may depend not only on the flux values, but also on the flux shape (as pointed out in the preceding paragraph), these parameters may alternatively increase and decrease in accuracy. This suggests that error accumulation from time step to time step is negligible in comparison to the errors generated from the assumption that the flux behaves in a step-like manner. This explains why the accuracy in the 34 mesh point case increases after T = 1.68 seconds (see Tables 18 and 19).

4-3. Variation of EPS

Figure 13 shows the value of $KE_{nf}/EOK - 1$ versus time for the various EPS parameters studied. The only detectable differences occur when EPS = 10^{-3}. Tables 20 to 25 show values for various important output parameters. It can be seen that with EPS = 10^{-4}, results are obtained which differ by less than 1% compared to EPS = 10^{-6}. However, significant differences are

obtained with EPS = 10^{-3}. Figures 14 and 15 show two representative flux shapes at various times. These results indicate that 10^{-4} is the largest EPS which will give satisfactory convergence. However, this may not be true, as discussed below.

In section 2-3-6, it was argued that if the iterations are converging too slowly, Equation 2-35 could be satisfied even if proper convergence has not been obtained. The satisfaction of Equation 2-35 at every point in the reactor would automatically terminate the calculation resulting in a flux shape which is inaccurate. Table 26 shows the total number of iterations for each time step. Immediately apparent is the drastic reduction in the number of iterations for EPS = 10^{-3}. The reason for this drastic reduction can be explained by considering that KE was held constant for five iterations before it was allowed to vary by the method described in section 2-3-6. This caused the convergence to proceed too slowly, terminating the iteration procedure before KE was given a chance to change its value. This is considered to be the prime reason for the inaccuracy obtained with EPS = 10^{-3}. Garvey[7] has suggested that a further reduction in computing time for negligible loss in accuracy could be obtained by setting EPS = 10^{-2} but ensuring that the iteration count has a minimum value which has been empirically determined to give satisfactory results. Furthermore, KE should be given a chance to vary by the method described in section 2-3-6.

5. CONCLUSIONS

1. The study of the length of the time step met with difficulty due to smeared representation of the shut-off rods. Further study with smaller mesh spacings is necessary to determine optimum time steps. Smearing effects should be studied in parallel.

2. Preliminary evidence suggests that interpolating the thermal flux when calculating integral quantities may decrease the number of mesh points needed for satisfactory convergence.

3. A value of EPS = 10^{-4} was sufficient for satisfactory convergence of the solution. The possibility of increasing EPS by at least an order of magnitude requires further study.

6. SUGGESTIONS FOR FURTHER WORK

From a cost point of view, the three parameters investigated in this work are the most important of all the input parameters, and their optimization can reduce computer time considerably. The choice of time step and number of mesh points are related, since if smaller time steps and fewer mesh points are used, smearing of SOR properties may be necessary. Hence, it is important to study the effects of smearing on the results. It may also be useful to continue the study of EPS by fixing the minimum number of iterations performed for each case. A study of the Liebmann acceleration parameter may prove fruitful in lowering computer costs.

From an accuracy point of view, it would be useful to study the effects of small errors on the experimentally measured physics and engineering variables which are fed into the calculation. Some examples of these are cross sections, the number of delayed neutron groups, errors in the total and individual delayed neutron fractions, errors in the voiding rate and errors in the SOR drop rates.

7. TABLES

TABLE 1

Initial Material Properties
for 1-D Reactor

Material Property	Regions 1 and 4	Regions 2 and 3
D_1 cm	1.2	1.2
D_2 cm	.9	.9
Σ_{a1} cm^{-1}	.001	.001
Σ_{a2} cm^{-2}	.004	.004
$\nu\Sigma_f$ cm^{-1}	.00430439	.00483891
Σ_{12} cm^{-1}	.008	.008
v_1 cm/sec	$.714 \times 10^7$	$.714 \times 10^7$
v_2 cm/sec	$.273 \times 10^6$	$.273 \times 10^6$

TABLE 2

Delayed Neutron Data
Note that $\beta = .00582$

Group	β_j	λ_j (sec^{-1})
1	.000295	.000612
2	.001165	.03155
3	.001033	.1218
4	.00235	.3175
5	.000780	1.389
6	.000197	3.784

TABLE 3

Incremental Shut-Off Rod Properties

Properties	Value cm^{-1}
$\Delta\Sigma_{tr}^{2}$	0
$\Delta\Sigma_{tr}^{1}$	-.733589E-3
$\Delta\Sigma_{a1}$	.5158992E-3
$\Delta\Sigma_{a2}$	.0039190188
$\Delta\nu\Sigma_{f}$	.5417969E-3
$\Delta\Sigma_{12}$	0

TABLE 4

Data for 20 cm Time Step

Case	Time (sec)	ρ' (t) (mk)	Distance of Rods (cm)
2	0.0	0.0	0
4	.06	1.0	0
6	.13	2.0	0
8	.19	3.0	0
10	.25	4.0	0
12	.36	5.0	0
14	.65	6.0	0
16	.68	6.075	20
18	.77	6.4	40
20	.835	6.6	60
22	.9	6.825	80
24	.97	7.05	100
26	1.03	7.25	120
28	1.08	7.425	140
30	1.14	7.6	140
32	1.195	7.825	180
34	1.25	8.0	200
36	1.295	8.15	220
38	1.35	8.375	240
40	1.4	8.5	260
42	1.44	8.625	280
44	1.49	8.8	300
46	1.54	8.95	320
48	1.58	9.125	340
50	1.63	9.275	360
52	1.68	9.45	380
54	1.72	9.575	400
56	1.77	9.75	420
58	1.825	9.925	440
60	1.88	10.125	460
62	1.925	10.2	480
64	1.97	10.25	500
66	2.01	10.275	520
68	2.14	10.375	540
70	2.3	10.5	560
72	2.5	10.65	570

TABLE 5

Data for 10 cm Time Step

Case	Time (sec)	$\rho'(t)$ (mk)	Distance of Rod (cm)	Case	Time	$\rho'(t)$	Distance of Rod (cm)
2	0.0	0.0	0	70	1.35	8.325	240
4	.06	1.0	0	72	1.37	8.4	250
6	.12	1.8	0	74	1.40	8.5	260
8	.18	2.9	0	76	1.42	8.55	270
10	.24	3.75	0	78	1.44	8.625	280
12	.30	4.75	0	80	1.46	8.7	290
14	.36	5.0	0	82	1.49	8.8	300
16	.42	5.2	0	84	1.51	8.875	310
18	.48	5.4	0	86	1.54	8.95	320
20	.54	5.6	0	88	1.56	9.025	330
22	.60	5.8	0	90	1.58	9.125	340
24	.63	5.925	10	92	1.6	9.175	350
26	.68	6.075	20	94	1.63	9.275	360
28	.72	6.2	30	96	1.65	9.35	370
30	.77	6.4	40	98	1.68	9.45	380
32	.8	6.5	50	100	1.7	9.5	390
34	.835	6.6	60	102	1.72	9.575	400
36	.86	6.75	70	104	1.75	9.675	410
38	.9	6.825	80	106	1.77	9.75	420
40	.94	6.95	90	108	1.8	9.85	430
42	.97	7.05	100	110	1.825	9.925	440
44	1.0	7.15	110	112	1.85	10.025	450
46	1.03	7.25	120	114	1.88	10.125	460
48	1.05	7.325	130	116	1.9	10.175	470
50	1.08	7.425	140	118	1.925	10.2	480
52	1.11	7.525	150	120	1.95	10.225	490
54	1.14	7.6	160	122	1.97	10.25	500
56	1.17	7.725	170	124	1.99	10.26	510
58	1.195	7.825	180	126	2.01	10.275	520
60	1.22	7.9	190	128	2.07	10.325	530
62	1.25	8.0	200	130	2.14	10.375	540
64	1.27	8.075	210	132	2.21	10.425	550
66	1.295	8.15	220	134	2.3	10.5	560
68	1.33	8.275	230	136	2.5	10.65	570

TABLE 6

Data for 5 cm Time Step

Case	Time (sec)	$\rho'(t)$ (mk)	Distance of Rod (cm)
98	1.67	9.425	375
100	1.68	9.45	380
102	1.69	9.475	385
104	1.7	9.5	390
106	1.71	9.55	395
108	1.72	9.575	400
110	1.74	9.64	405
112	1.75	9.675	410
114	1.76	9.7	415
116	1.77	9.75	420
118	1.78	9.78	425
120	1.8	9.85	430
122	1.81	9.875	435
124	1.825	9.925	440
126	1.84	9.975	445
128	1.85	10.025	450
130	1.86	10.05	455
132	1.87	10.075	460
134	1.885	10.125	465
136	1.9	10.175	470
138	1.91	10.19	475
140	1.925	10.2	480
142	1.94	10.21	485
144	1.95	10.225	490
146	1.96	10.24	495
148	1.97	10.25	500
150	1.98	10.25	505
152	1.99	10.26	510
154	2.0	10.27	515
156	2.01	10.275	520
158	2.04	10.3	525
160	2.07	10.325	530
162	2.10	10.34	535
164	2.13	10.36	540
166	2.16	10.38	545
168	2.2	10.4	550
170	2.24	10.44	555
172	2.28	10.48	560
174	2.36	10.55	565
176	2.5	10.65	570

TABLE 7

Data for 2.5 cm Time Step

Case	Time (sec)	$\rho'(t)$ (mk)	Distance of Rod (cm)	Case	Time (sec)	$\rho'(t)$ (mk)	Distance of Rod (cm)
110	1.73	9.6	402.5	178	1.945	10.218	487.5
112	1.74	9.64	405	180	1.95	10.225	490
114	1.745	9.66	407.5	182	1.955	10.233	492.5
116	1.75	9.675	410	184	1.96	10.24	495
118	1.755	9.7	412.5	186	1.965	10.245	497.5
120	1.76	9.7	415	188	1.97	10.25	500
122	1.765	9.725	417.5	190	1.975	10.25	502.5
124	1.77	9.75	420	192	1.98	10.25	505
126	1.775	9.76	422.5	194	1.985	10.255	507.5
128	1.782	9.78	425	196	1.99	10.26	510
130	1.79	9.825	427.5	198	1.995	10.265	512.5
132	1.8	9.85	430	200	2.0	10.27	515
134	1.805	9.87	432.5	202	2.01	10.275	517.5
136	1.81	9.9	435	204	2.02	10.29	520
138	1.818	9.925	437.5	206	2.03	10.3	522.5
140	1.825	9.925	440	208	2.04	10.3	525
142	1.832	9.95	442.5	210	2.055	10.31	527.5
144	1.84	9.975	445	212	2.07	10.325	530
146	1.845	10.0	447.5	214	2.085	10.33	532.5
148	1.85	10.025	450	216	2.1	10.34	535
150	1.855	10.035	452.5	218	2.115	10.35	537.5
152	1.86	10.05	455	220	2.13	10.36	540
154	1.865	10.075	457.5	222	2.145	10.37	542.5
156	1.87	10.075	460	224	2.16	10.38	545
158	1.878	10.1	462.5	226	2.19	10.39	547.5
160	1.885	10.125	465	228	2.2	10.4	550
162	1.893	10.15	467.5	230	2.23	10.44	552.5
164	1.9	10.175	470	232	2.24	10.45	555
166	1.905	10.19	472.5	234	2.26	10.465	557.5
168	1.91	10.19	475	236	2.28	10.48	560
170	1.9175	10.195	477.5	238	2.34	10.51	562.5
172	1.925	10.2	480	240	2.37	10.55	565
174	1.9325	10.205	482.5	242	2.43	10.6	567.5
176	1.94	10.21	485	244	2.5	10.65	570

TABLE 8

The Geometry of the 34 Mesh Point Reactor

Mesh Point Number	Position (cm)
1	10
2	25
3	35
4	50
5	70
6	90
7	110
8	130
9	145
10	155
11	170
12	190
13	210
14	230
15	250
16	270
17	290
18	310
19	330
20	350
21	370
22	390
23	410
24	430
25	445
26	455
27	470
28	490
29	510
30	530
31	550
32	565
33	575
34	590

TABLE 9

$$\int \nu\Sigma_f \psi_2(x,t)\, dV$$
REACTOR

$$\left[\int \nu\Sigma_f \psi_2(0)\, dV = 1.667308\right]$$
REACTOR

Time (sec)	Time Step = 20 cm, No Smearing	Time Step = 10 cm, No Smearing	Time Step = 5 cm, Smearing	Time Step = 2.5 cm, Smearing
.06	1.6681	1.6681		
.36	1.6717	1.6717		
.68	1.6718	1.6722		
.97	1.6824	1.6821		
1.44	1.6424	1.6425		
1.77	1.5245	1.5244	1.5244	1.5243
1.825	1.5296	1.5293	1.5295	1.5295
1.85		1.5405	1.5407	1.5407
1.88	1.5600	1.5599	1.5592	1.5594
1.925	1.6231	1.6236	1.6251	1.6255
1.97	1.7207	1.7206	1.7211	1.7213
2.01	1.82725	1.8243	1.8228	1.8128
2.14	1.8735	1.8704	1.8682	1.8693
2.5	1.8408	1.8402	1.8406	1.8399

TABLE 10

Relative Maximum Shape Function and its Position

Time (sec)	TS=20 cm No Smearing	Position (cm)	TS=10 cm No Smearing	Position (cm)	TS=5 cm Smearing	Position (cm)	TS=2.5 cm Smearing	Position (cm)
1.77	2.4632	515	2.4617	515	2.4623	515	2.4627	515
1.825	2.6328	525	2.6325	525	2.6333	525	2.6338	525
1.85			2.7541	525	2.7519	525	2.7517	525
1.925	3.1836	535	3.1633	535	3.136	535	3.133	535
1.97	3.4524	545	3.3940	545	3.343	545	3.320	545
2.01	3.375	555	3.2715	555	3.204	555	3.187	555
2.5	1.4513	505	1.4660	505	1.459	505	1.470	505

TABLE 11

The Shape Function at Two Positions in the Reactor

Time (sec)	TS = 20 cm No Smearing		TS = 10 cm No Smearing		TS = 5 cm Smearing		TS = 2.5 cm Smearing	
	ψ_2(105 cm)	ψ_2(495 cm)	ψ_2(105 cm)	ψ_2(495 cm)	ψ_2(105 cm)	ψ_2(495 cm)	ψ_2(105 cm)	ψ_2(495 cm)
.06	.979	1.022	.979	1.022				
.36	.756	1.246	.752	1.250				
.68	.564	1.441	.538	1.467				
.97	.043	1.946	.042	1.947				
1.44	.001	2.068	.001	2.068				
1.77	.002	2.431	.002	2.431	.002	2.431	.002	2.431
1.825	.006	2.538	.005	2.539	.006	2.539	.006	2.539
1.85			.010	2.581	.011	2.58	.011	2.580
1.925	.056	2.432	.059	2.431	.067	2.421	.067	2.420
1.97	.118	1.603	.127	1.607	.136	1.605	.140	1.603
2.01	.229	1.235	.238	1.248	.247	1.254	.240	1.273
2.5	.538	1.451	.525	1.466	.531	1.459	.521	1.470

TABLE 12

$$\frac{\text{LEAKAGE}}{\text{PRODUCTION}} * 10^3 \text{ (mk)}$$

Time (sec)	TS = 20 cm No Smearing	TS = 10 cm No Smearing	TS = 5 cm Smearing	TS = 2.5 cm Smearing
1.77	23.90	23.84	23.85	23.86
1.825	27.22	27.18	27.21	27.23
1.925	37.75	37.30	36.84	36.79
1.97	43.86	42.75	41.89	41.52
2.01	47.00	45.17	44.10	43.46
2.5	28.86	28.85	28.79	28.84

TABLE 13

$\rho(t)$ (mk)

Time (sec)	TS = 20 cm No Smearing	TS = 10 cm No Smearing	TS = 5 cm Smearing	TS = 2.5 cm Smearing
.06	.50989	.50989		
.36	3.0426	3.069		
.68	3.3736	3.4898		
.97	4.1117	4.2313		
1.44	5.8662	5.9045		
1.75		- 6.8119	- 7.0268	- 7.0117
1.77	- 11.147	- 11.459	-11.559	-11.54
1.825	- 24.967	- 25.798	-26.415	-26.75
1.85		- 37.701	-39.848	-40.746
2.01	-366.77	-415.02		
2.5	-812.93	-812.99		

TABLE 14

Table of Amplitudes

Time (sec)	Time Step = 20 cm No Smearing	Time Step = 10 cm No Smearing	Time Step = 5 cm Smearing	Time Step = 2.5 cm Smearing
.06	1.015	1.015		
.36	1.4249	1.4361		
.68	2.1630	2.1647		
.97	2.4681	2.4894		
1.44	5.5176	5.6953		
1.75		3.4208	3.4062	3.4007
1.77	2.4934	2.6365	2.5998	2.5921
1.825	0.86476	0.92213	0.85784	0.85272
1.85		0.48642	0.45007	0.44104
1.88	0.23482	0.23005		
2.01	0.0237	0.0214		
2.3	0.00956	0.00936		
2.5	0.00833	0.00856		

TABLE 15

Table of: $\frac{\int \nu\Sigma_f \, \psi_2(t) \, dV}{\int \nu\Sigma_f \, \psi_2(0) \, dV}$

Time	34 Mesh Points	60 Mesh Points	% Difference
.06	1.000526	1.000475	< .03
.25	1.002106	1.00203	< .03
.65	1.00342	1.00341	< .03
.77	1.00447	1.00455	< .03
.9	1.00684	1.00851	< .03
1.03	1.00912	1.00911	< .03
1.14	1.00807	1.00803	< .03
1.35	.99789	.99754	< .03
1.54	.96657	.96593	< .03
1.68	.93060	.93036	< .03
1.77	.91305	.91435	.14
2.01	1.09440	1.09593	.14
2.5	1.10546	1.10406	.13

TABLE 16

Form Factor

Time	34 Mesh Points	60 Mesh Points	% Difference
.06	.5924	.5955	.52
.25	.5234	.5262	.53
.65	.4352	.4380	.64
.77	.3654	.3667	.36
.9	.3212	.3227	.64
1.03	.3103	.3115	.39
1.14	.3058	.3070	.39
1.35	.2968	.2976	.04
1.54	.2777	.2776	.64
1.68	.2525	.2509	.53
1.77	.2270	.2258	2.7
2.01	.1924	.1975	1.4
2.5	.4594	.4529	

TABLE 17

$\frac{\text{Maximum Flux (t)}}{\text{Initial Maximum}}$ and Position

Time (sec)	34 Mesh Points	Position (cm)	60 Mesh Points	Position (cm)	% Difference
.06	1.0216	490	1.0215	495	.01
.25	1.1581	490	1.1577	495	.03
.65	1.3946	490	1.3930	495	.11
.77	1.6625	490	1.6656	495	.19
.9	1.8961	490	1.9000	495	.21
1.03	1.9670	490	1.9694	495	.12
1.14	1.9940	490	1.9963	495	.12
1.35	2.0335	490	2.0379	495	.23
1.54	2.1054	490	2.1154	495	.46
1.68	2.2296	490	2.2542	495	1.1
1.77	2.4328	510	2.4623	505	1.2
2.01	3.4410	550	3.3738	555	2.0
2.5	1.4553	490	1.4821	495	1.8

TABLE 18

$\rho(t)$ (mk)

Time (sec)	34 Mesh Points	60 Mesh Points	% Difference
.06	.50994	.50989	.01
.25	2.2888	2.2872	.07
.65	3.972	3.9649	.18
.77	2.8627	2.847	.55
.9	3.6204	3.5902	.84
1.03	4.5145	4.4774	.83
1.14	5.0657	5.0259	.79
1.35	5.9128	5.8554	.98
1.54	5.4503	5.3084	2.7
1.68	1.1903	.72379	64.5
1.77	- 9.8639	- 11.147	13.0
2.01	-348.3	-366.77	5.3
2.5	-813.67	-812.93	.09

TABLE 19

Table of Amplitudes

Time	34 Mesh Points	60 Mesh Points	% Difference
.06	1.0150	1.0150	0
.25	1.2137	1.2136	.01
.65	2.1060	2.1033	.13
.77	2.2428	2.2195	1.05
.9	2.3317	2.3046	1.2
1.03	2.7042	2.6706	1.3
1.14	3.202	3.1571	1.4
1.35	4.7504	4.6573	2.0
1.54	6.6006	6.387	3.3
1.68	6.0059	5.6125	7.0
1.77	2.8475	2.4934	14.2
2.01	.025591	.023738	7.8
2.5	.0084691	.0083315	1.7

TABLE 20

Table of $\int \nu \Sigma_f \psi_2 dV$

Time	EPS = 10^{-3}	EPS = 10^{-4}	EPS = 10^{-5}	EPS = 10^{-6}
.06	1.668117	1.668065	1.668105	1.668094
.12	1.668675	1.668706	1.66875	1.668752
.18	1.669225	1.66965	1.669687	1.669695
.24	1.669699	1.670414	1.670466	1.670475
.30	1.670523	1.671355	1.671417	1.671426
.36	1.670808	1.671654	1.67173	1.671738
.42	1.671074	1.67192	1.671996	1.672004
.48	1.671341	1.672177	1.672252	1.672260
.54	1.671603	1.672429	1.672503	1.672511
.60	1.67187	1.672681	1.672754	1.672762
.63	1.671595	1.672541	1.672536	1.672528
.68	1.671018	1.672091	1.672163	1.672157
2.10	1.8633	1.863642	1.863681	1.863721
2.16	1.86696	1.863642	1.867389	1.867423
2.26	1.854697	1.854663	1.854678	1.85479
2.37	1.844506	1.843993	1.843965	1.844163
2.43	1.842264	1.841575	1.841528	1.841755
2.5	1.840864	1.839758	1.839672	1.83993

TABLE 21

Maximum Flux and Its Position

Time (sec)	EPS=10^{-3}	Position (cm)	EPS=10^{-4}	Position (cm)	EPS=10^{-5}	Position (cm)	EPS=10^{-6}	Position (cm)
.06	1.001832	505	1.017887	505	1.02147	505	1.021866	505
.12	1.005318	505	1.04658	505	1.052544	505	1.053273	505
.18	1.019321	505	1.089503	505	1.097285	505	1.098199	505
.24	1.042466	505	1.137199	505	1.146413	505	1.14742	505
.30	1.0878	505	1.192846	505	1.202977	505	1.20403	505
.36	1.125479	505	1.238622	505	1.249168	505	1.250238	505
.42	1.157469	505	1.276349	505	1.287056	505	1.288127	505
.48	1.187137	505	1.309481	505	1.32027	505	1.321337	505
.54	1.214929	505	1.339553	505	1.350325	505	1.351377	505
.60	1.241578	505	1.366688	505	1.377331	505	1.378364	505
.63	1.276509	505	1.391820	505	1.398831	505	1.398553	505
.68	1.352539	505	1.460670	505	1.467693	505	1.46651	505
2.10	2.546442	565	2.590178	565	2.59397	565	2.585963	565
2.16	2.090462	565	2.132719	565	2.136289	565	2.128669	565
2.26	1.480103	575	1.514264	575	1.517136	575	1.511009	575
2.37	1.438346	505	1.473037	505	1.475859	505	1.469852	505
2.43	1.435128	505	1.470315	505	1.473197	505	1.467075	505
2.5	1.437269	505	1.473311	505	1.476349	505	1.470124	505

TABLE 22

$$\text{Form Factor} = \frac{\int \nu\Sigma_f \psi_2(t)\, dV}{\psi_2^{max}(t) \int \nu\Sigma_f dV}$$

Time	EPS = 10^{-3}	EPS = 10^{-4}	EPS = 10^{-5}	EPS = 10^{-6}
.06	.60703	.59743	.59535	.59512
.12	.60512	.58128	.57800	.57760
.18	.59701	.55869	.55474	.55428
.24	.58392	.53550	.53122	.53075
.30	.55986	.51081	.50653	.50609
.36	.54121	.49202	.48789	.48747
.42	.52633	.47755	.47360	.47321
.48	.51326	.46554	.46176	.46139
.54	.50160	.45516	.45155	.45120
.60	.49091	.44619	.44276	.44243
.63	.47740	.43810	.43590	.43598
.68	.45041	.41733	.41535	.41569
2.10	.26676	.26231	.26193	.26274
2.16	.32559	.31857	.31868	.31982
2.26	.45683	.44652	.44568	.44751
2.37	.46751	.45550	.45549	.45741
2.43	.46799	.45662	.45571	.45767
2.5	.46694	.45524	.45428	.45627

TABLE 23

$$\frac{\psi(x,t)}{\psi(x,0)}$$

Time (sec)	EPS = 10^{-3}		EPS = 10^{-4}		EPS = 10^{-5}		EPS = 10^{-6}	
	x = 105 cm	x = 495 cm	x = 105 cm	x = 495 cm	x = 105 cm	x = 495 cm	x = 105 cm	x = 495 cm
.06	.999	1.002	.983	1.018	.979	1.021	.979	1.022
.12	.996	1.005	.954	1.047	.948	1.053	.948	1.053
.18	.983	1.019	.912	1.090	.904	1.097	.903	1.098
.24	.960	1.042	.864	1.137	.855	1.146	.857	1.147
.30	.915	1.088	.809	1.193	.799	1.203	.798	1.204
.36	.878	1.125	.763	1.239	.753	1.249	.752	1.250
.42	.846	1.157	.726	1.276	.715	1.287	.702	1.288
.48	.816	1.187	.693	1.309	.682	1.320	.681	1.321
.54	.788	1.215	.663	1.340	.652	1.350	.651	1.351
.60			.636	1.367	.625	1.377	.624	1.378
.63	.728	1.277	.611	1.392	.604	1.399	.604	1.399
.68			.544	1.461	.537	1.468	.538	1.467
2.1			.357	1.310			.359	1.308
2.16			.416	1.380	.413	1.383	.418	1.378
2.26	.506	1.420	.473	1.453	.471	1.455	.476	1.450
2.37			.501	1.473			.504	1.470
2.43	.547	1.433	.513	1.470	.511	1.473	.516	1.467
2.5	.552	1.437	.518	1.473			.521	1.470

TABLE 24

REACTIVITY (ρ)

Time (sec)	EPS = 10^{-3}	EPS = 10^{-4}	EPS = 10^{-5}	EPS = 10^{-6}
.06	.500	.50746	.50967	.50989
.12	.903	.9373	.94307	.94365
.18	1.465	1.5671	1.5783	1.5795
.24	1.929	2.1083	2.1244	2.1261
.30	2.546	2.7904	2.8123	2.8146
.36	2.7716	3.0422	3.0665	3.069
.42	2.960	3.2554	3.2812	3.2838
.48	3.150	3.4644	3.4912	3.4939
.54	3.339	3.6712	3.6991	3.7019
.6		3.8756	3.9043	3.9071
.63	3.501	3.8795	3.9110	3.8765
.68		3.4634	3.4954	3.4898
2.1		-619.83		-620.22
2.16		-706.3	-706.06	-706.58
2.26	-780.7	-779.2	-779.08	-779.35
2.43	-809.8	-809.18	-809.13	-809.24
2.5	-813.6	-813.26		-813.3

TABLE 25

Table of Amplitudes

Time (sec)	EPS = 10^{-3}	EPS = 10^{-4}	EPS = 10^{-5}	EPS = 10^{-6}
.06	1.0147	1.0149	1.0150	1.0150
.12	1.0506	1.0520	1.0523	1.0523
.18	1.106	1.1112	1.112	1.112
.24	1.1802	1.1939	1.1954	1.1956
.30	1.277	1.3038	1.3065	1.3068
.36	1.3883	1.4315	1.4357	1.4361
.42	1.497	1.5590	1.5648	1.5654
.48	1.609	1.6913	1.6990	1.6998
.54	1.726	1.8319	1.8416	1.8426
.60	1.8462	1.9784	1.9905	1.9917
.63	1.9647	2.1271	2.1418	2.0675
.68	2.0313	2.2242	2.2413	2.1647
2.1	.012684	.013533	.013607	0.013363
2.16	.010777	.011457	.011517	.011318
2.26	.009320	.0098698	.0099182	.0097546
2.37	.0086969	.0091893	.0092328	.0090849
2.43	.008386	.0088498	.0088907	.008751
2.5	.008305	.0087596	.0087997	.008662

TABLE 26

Number of Iterations
(Case A + Case B)

Time (sec)	EPS = 10^{-3}	EPS = 10^{-4}	EPS = 10^{-5}	EPS = 10^{-6}
.06	5	106	262	472
.12	6	134	306	566
.18	16	163	372	645
.24	23	177	412	689
.30	44	199	448	727
.36	39	197	450	731
.42	35	190	444	727
.48	34	185	439	723
.54	33	182	437	720
.60	33	179	433	828
.63	40	202	433	423
.68	67	208	414	645
2.1	26	40	54	67
2.16	24	38	51	64
2.26	22	34	46	60
2.37	20	30	44	57
2.43	20	29	42	55
2.5	23	32	46	58

8. FIGURES

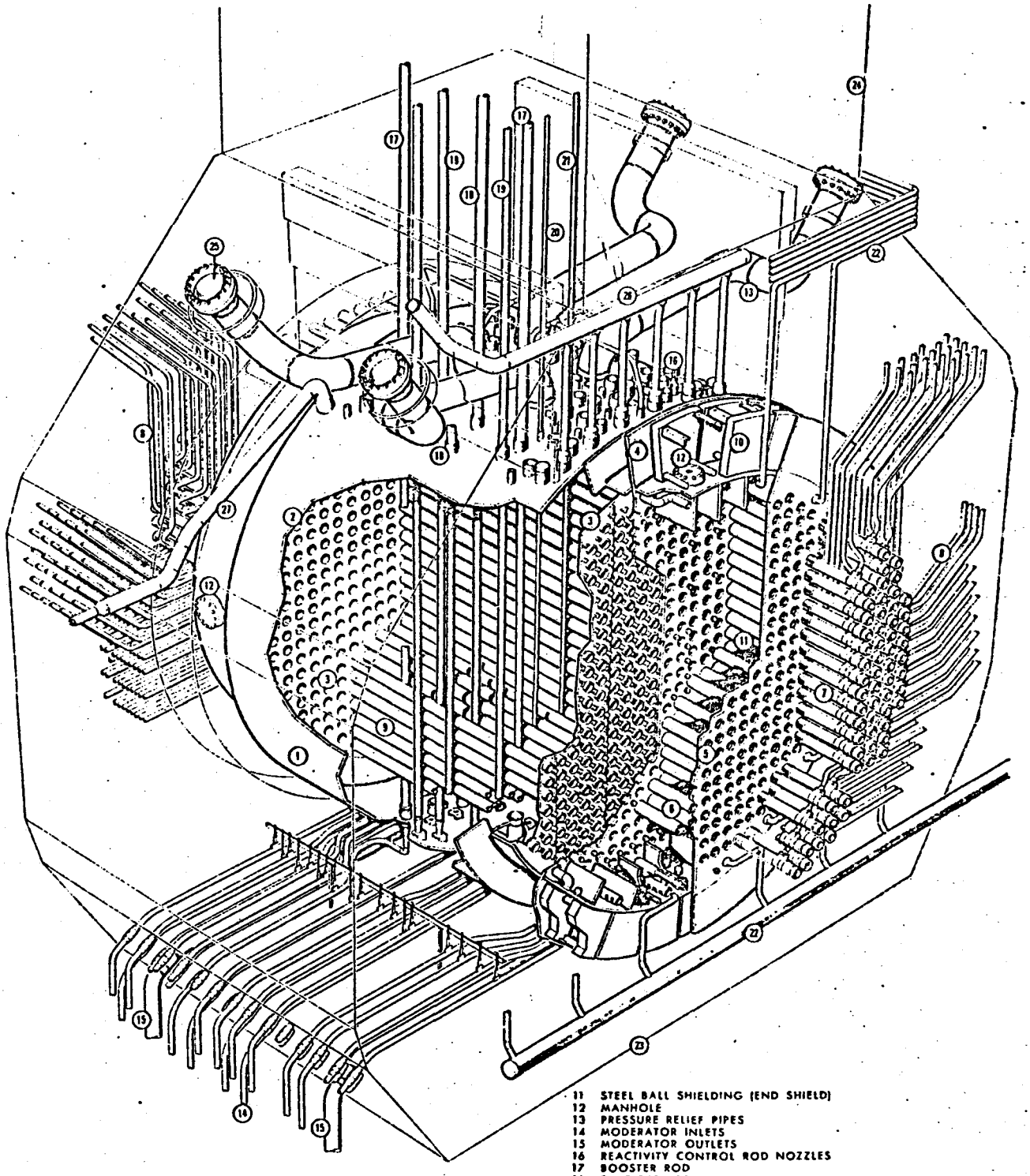

1 CALANDRIA
2 CALANDRIA SHELL
3 CALANDRIA SIDE TUBE SHEET
4 BAFFLE PLATE
5 FUELLING MACHINE SIDE TUBE SHEET
6 LATTICE TUBE
7 END FITTINGS
8 FEEDERS
9 CALANDRIA TUBES
10 SHIELD TANK SOLID SHIELDING
11 STEEL BALL SHIELDING (END SHIELD)
12 MANHOLE
13 PRESSURE RELIEF PIPES
14 MODERATOR INLETS
15 MODERATOR OUTLETS
16 REACTIVITY CONTROL ROD NOZZLES
17 BOOSTER ROD
18 SHUT-OFF ROD
19 ZONE CONTROL ROD
20 FLUX MONITOR
21 FLUX MONITOR AND POISON INJECTION
22 END SHIELD COOLING PIPING
23 SHIELD TANK
24 SHIELD TANK EXTENSION
25 RUPTURE DISC ASSEMBLY
26 MODERATOR INLET HEADER
27 MODERATOR OVERFLOW

FIGURE 1 REACTOR ASSEMBLY

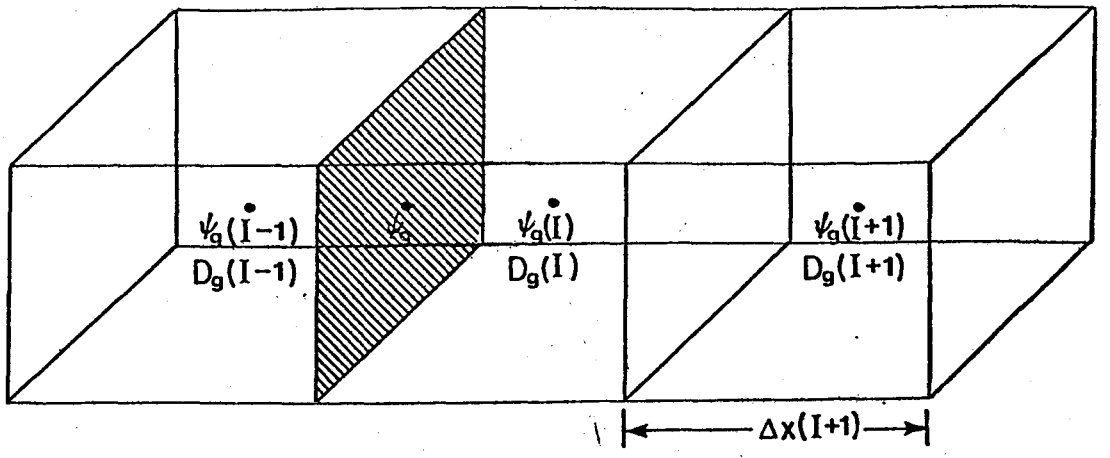

FIGURE 2 REPRESENTATIVE REACTOR CELL UNITS

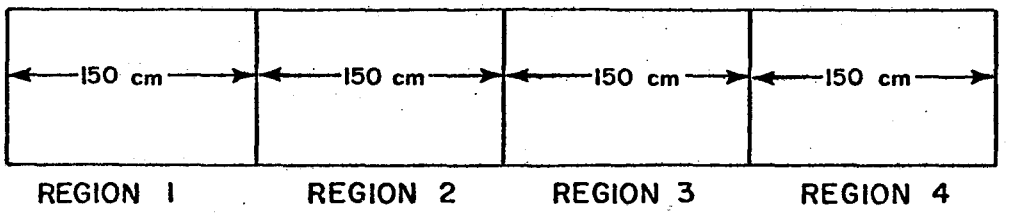

FIGURE 3 ONE DIMENSIONAL REACTOR MODEL USED IN THIS STUDY

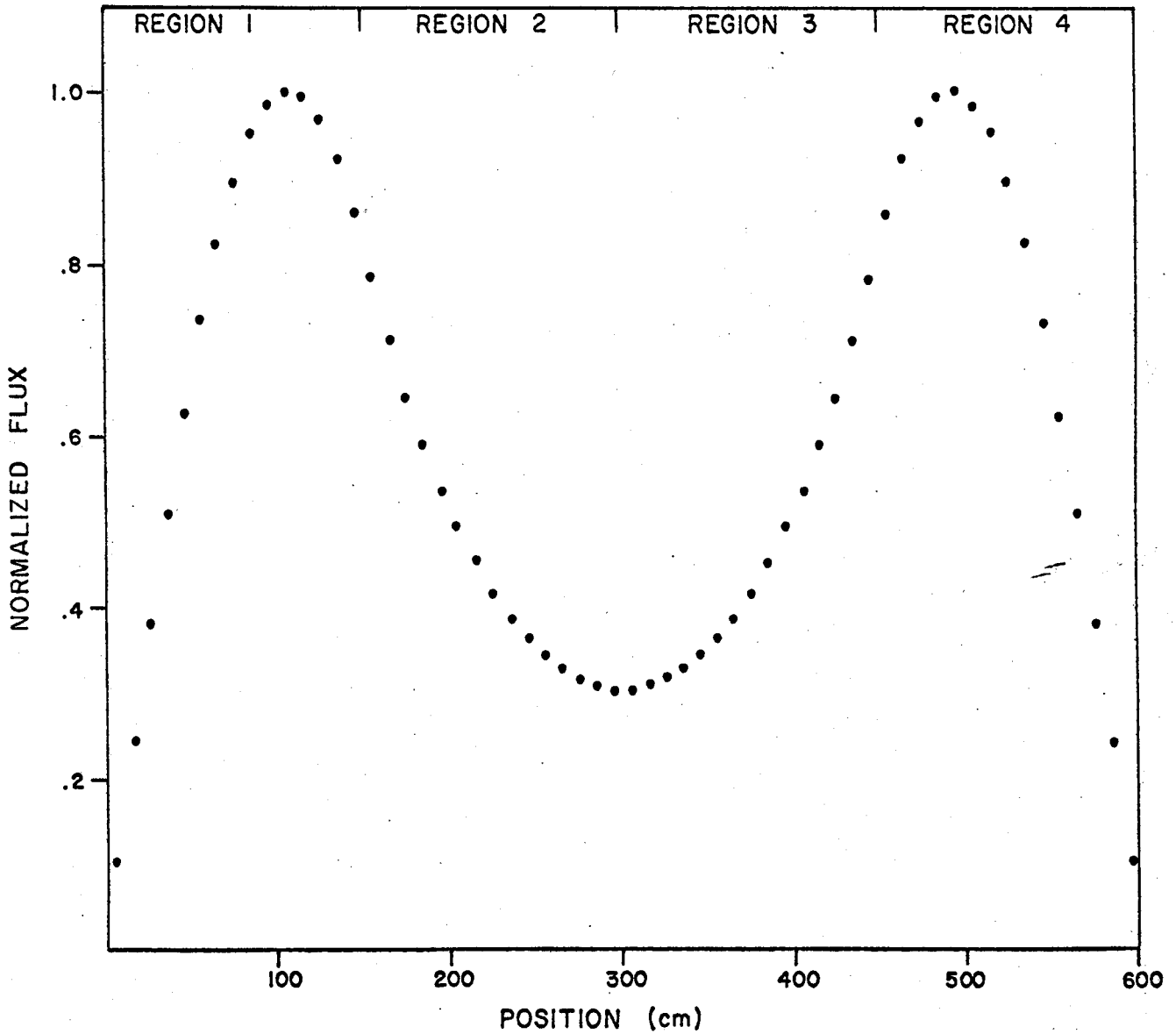

FIGURE 4 Normalized flux shape at t=0 showing neutronic decoupling.

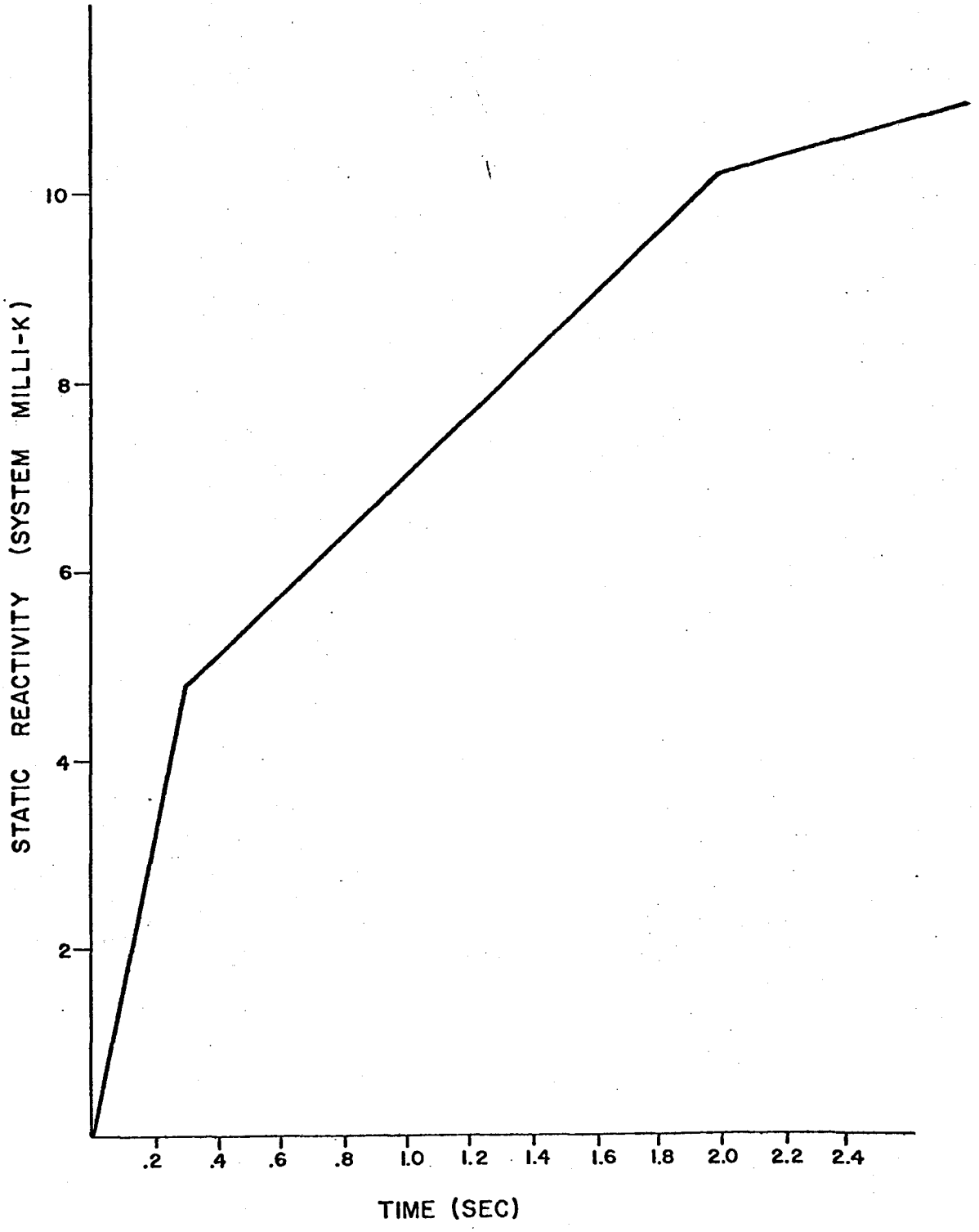

FIGURE 5 The LOC reactivity perturbation.

FIGURE 6

DISTANCE OF S.O.R. vs TIME

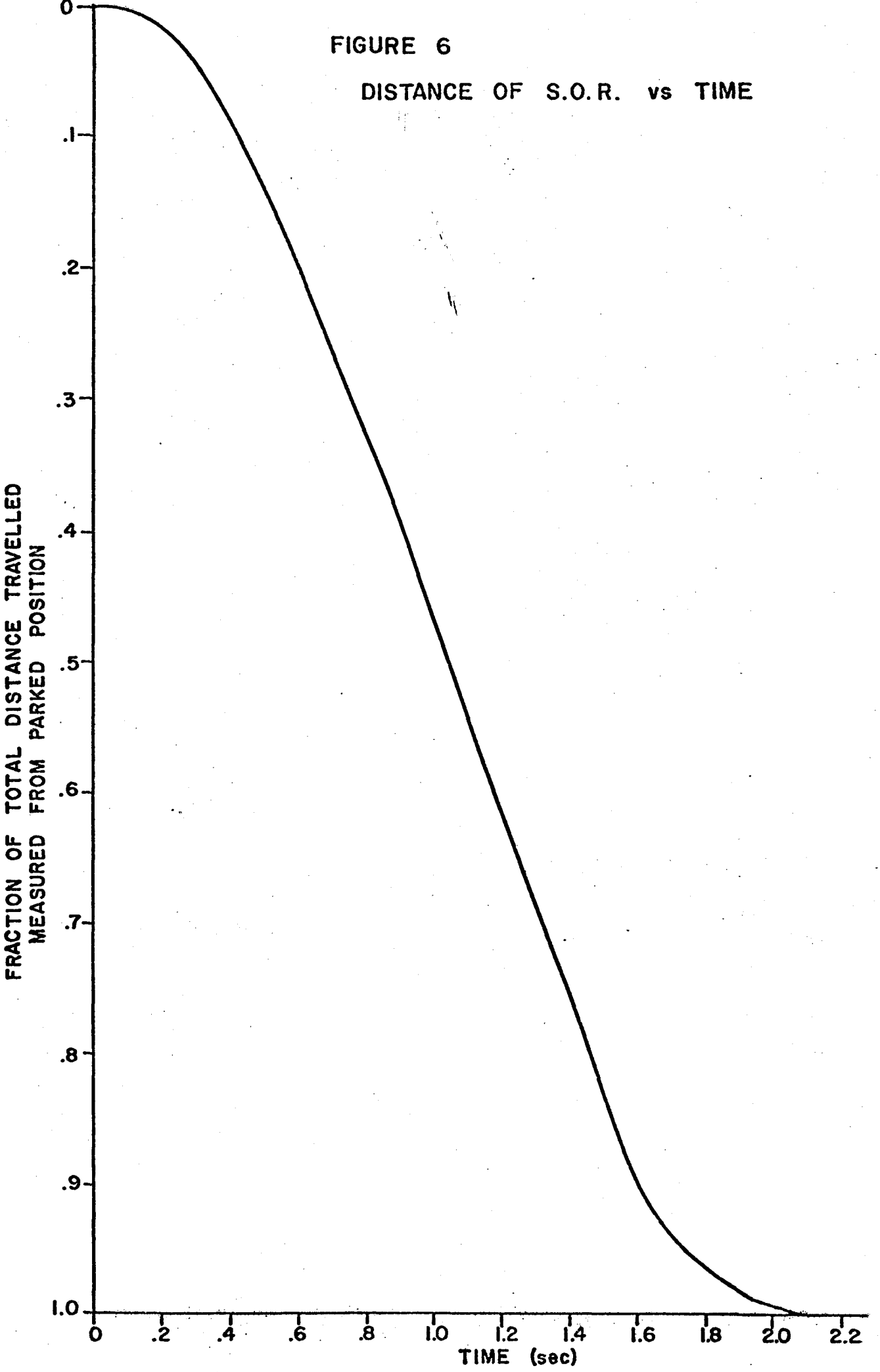

FIGURE 7 $\left(\frac{KE_{n_f}}{EOK} - 1\right) \times 10^{-3}$ vs TIME

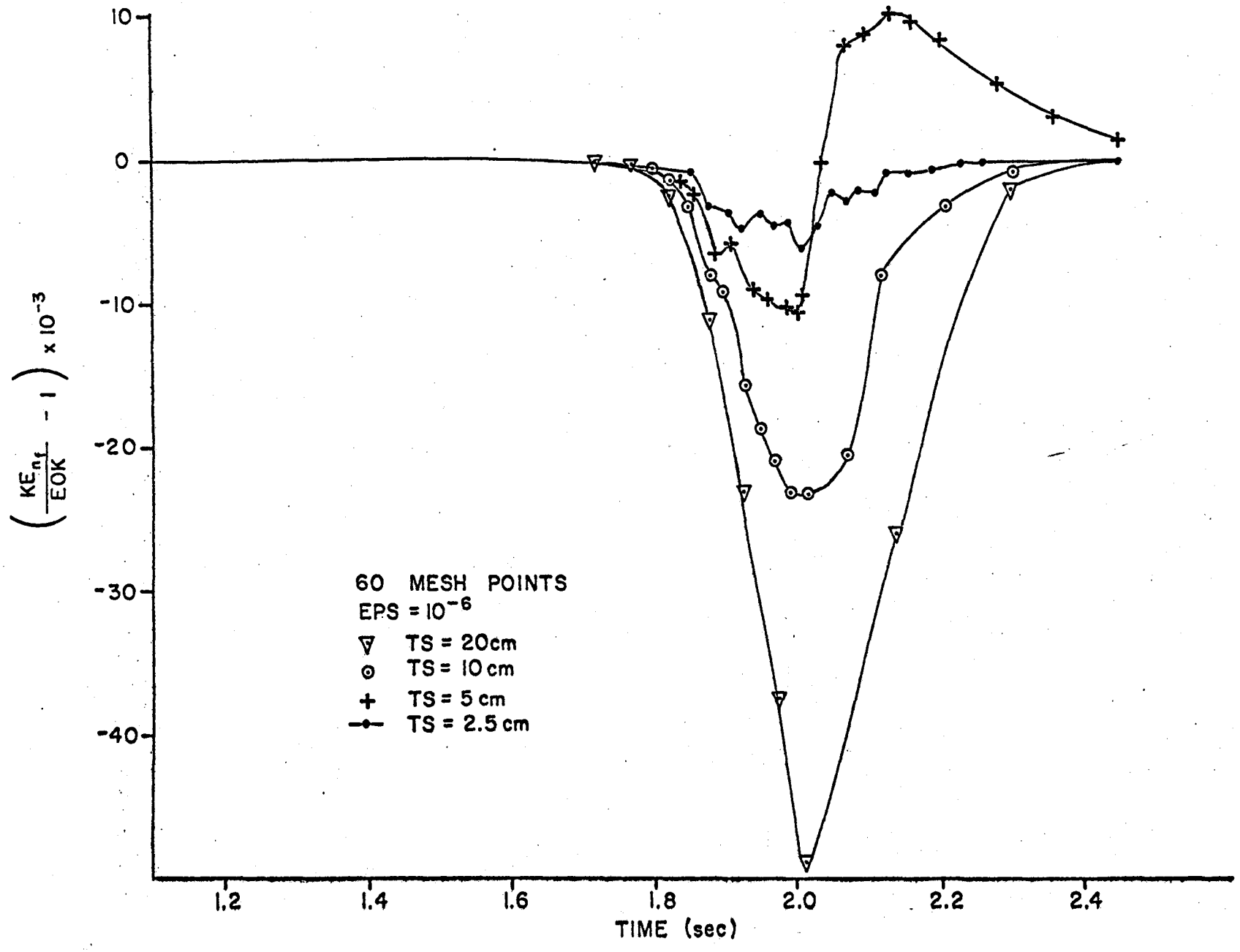

FIGURE 8 $10^3\left(\frac{KE_{nf}}{EOK} - 1\right)$ vs TIME

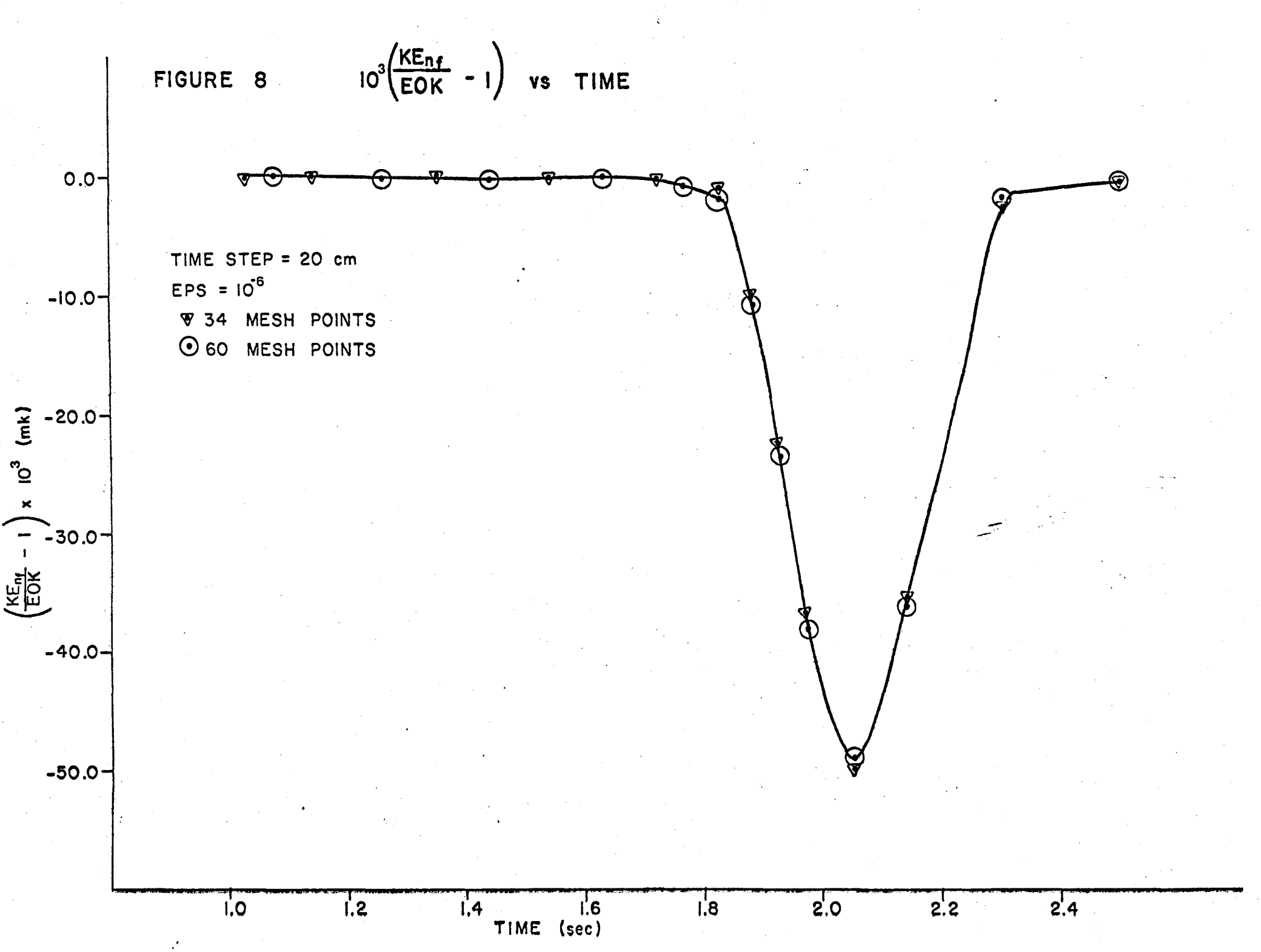

FIGURE 9 NORMALIZED FLUX vs DISTANCE

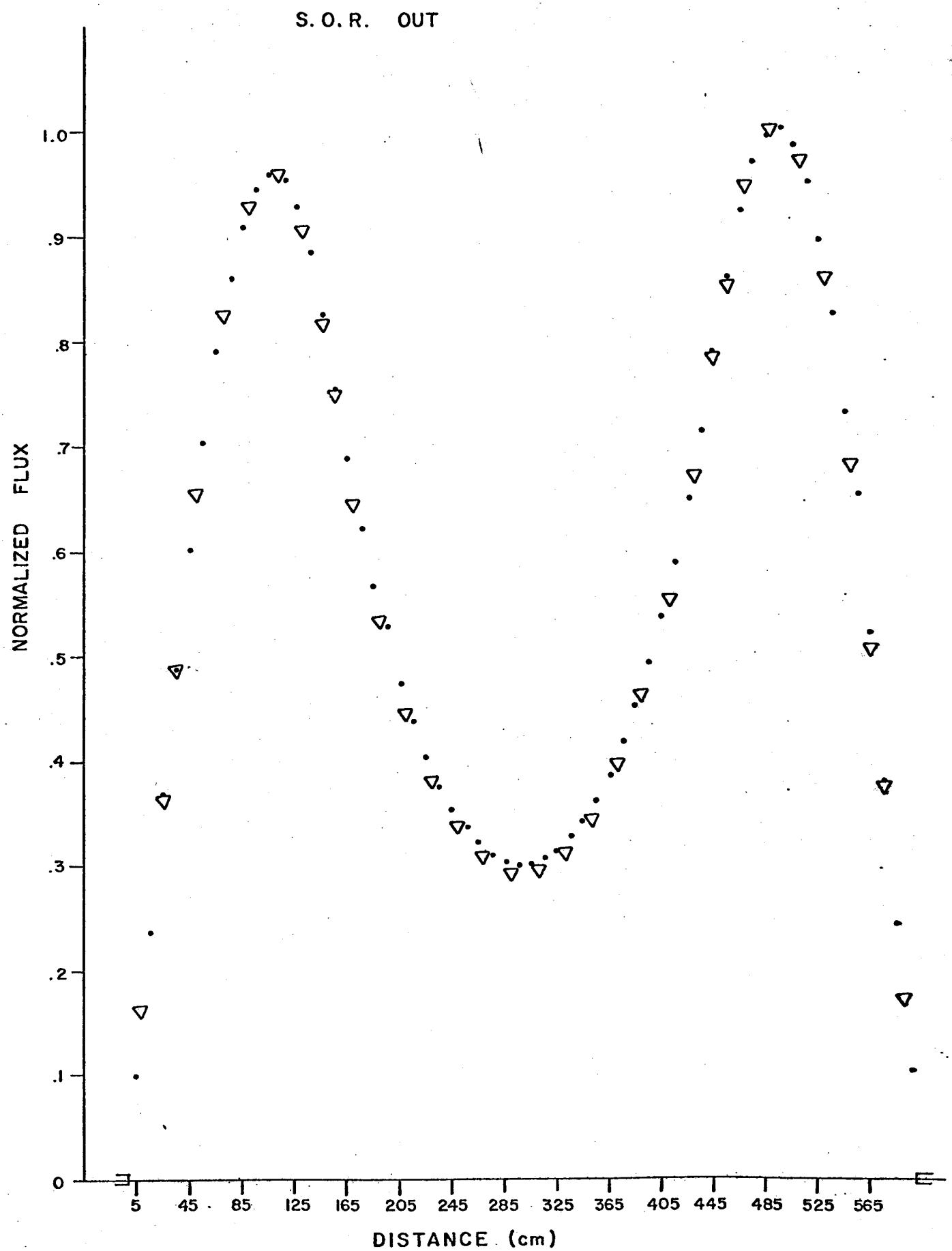

FIGURE 10 NORMALIZED FLUX vs DISTANCE

T = 1.68 sec

• 60 mesh points AMP = 5.6125
▽ 34 mesh points AMP = 6.0059

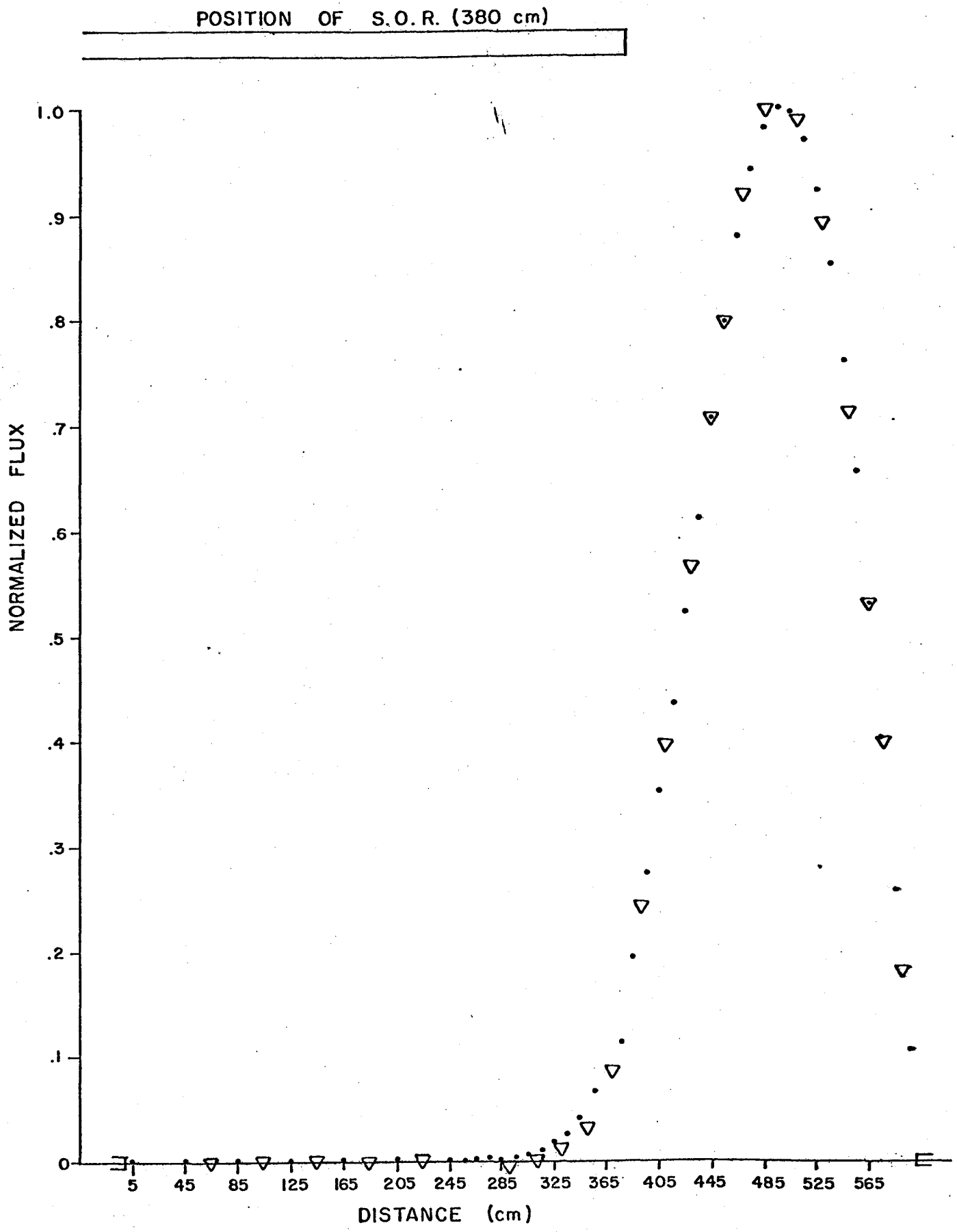

FIGURE II NORMALIZED FLUX vs DISTANCE

T = 2.01 sec

• 60 mesh points AMP = .023738

▽ 34 mesh points AMP = .025591

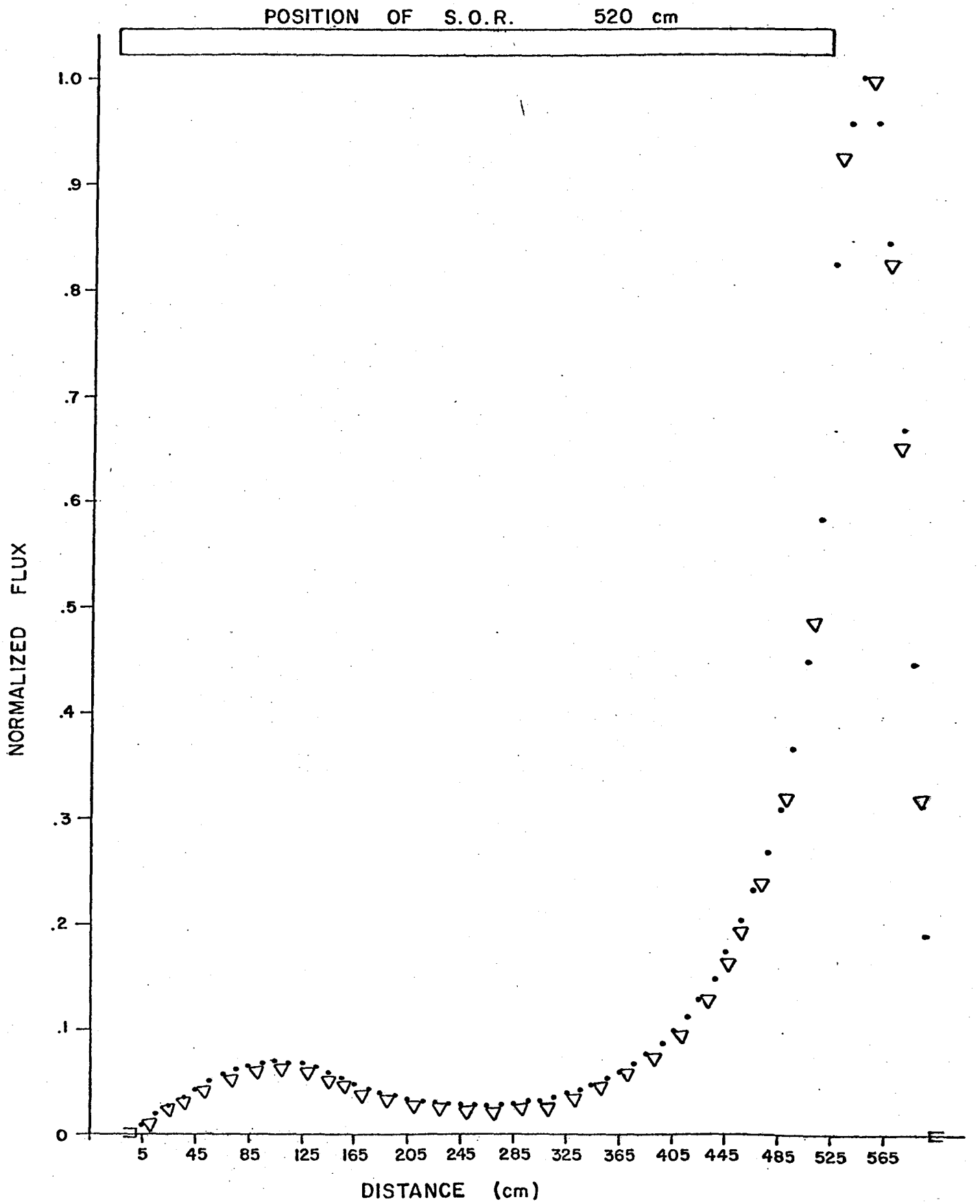

FIGURE 12 NORMALIZED FLUX vs DISTANCE

T = 2.5 sec

• 60 mesh points AMP = .0083315

▽ 34 mesh points AMP = .0084691

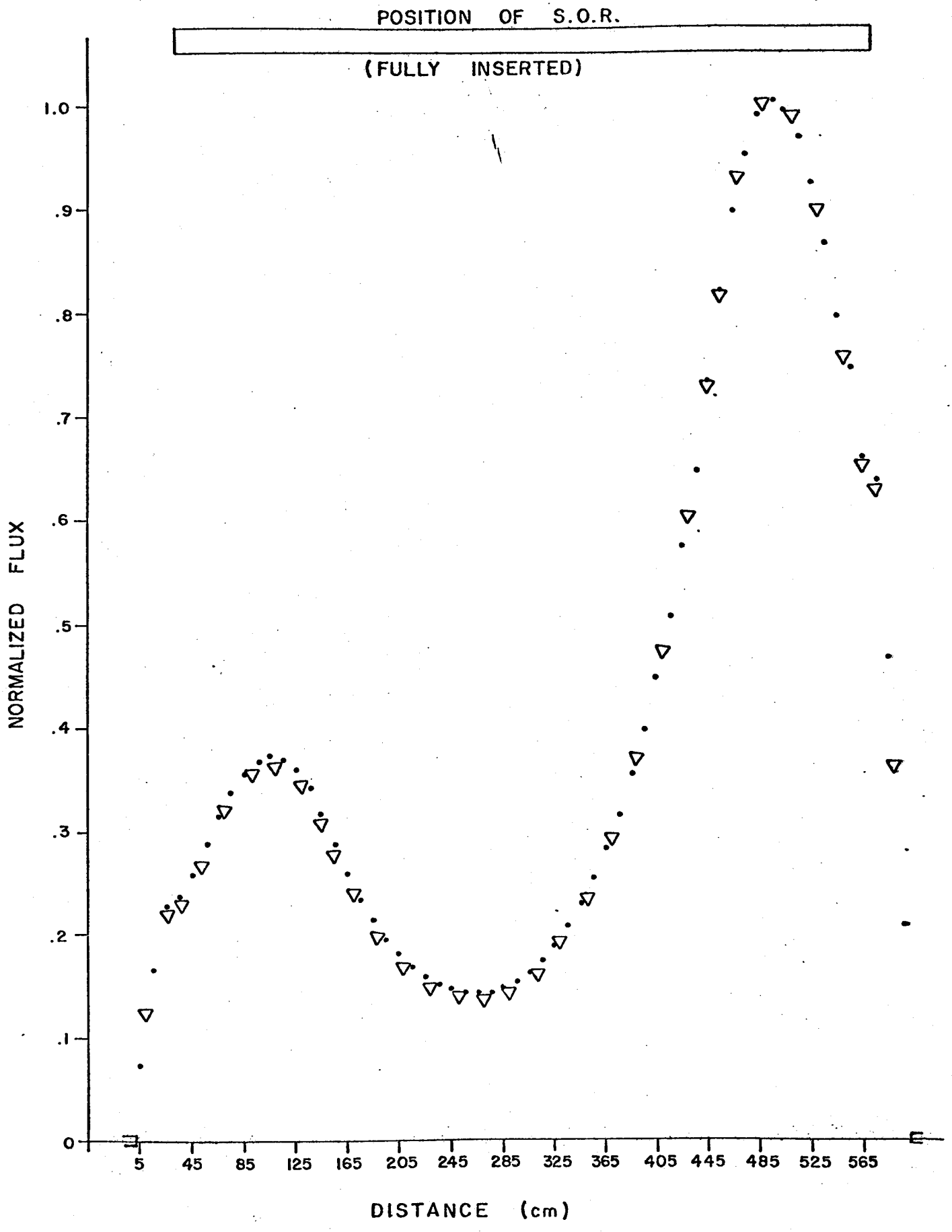

FIGURE 13

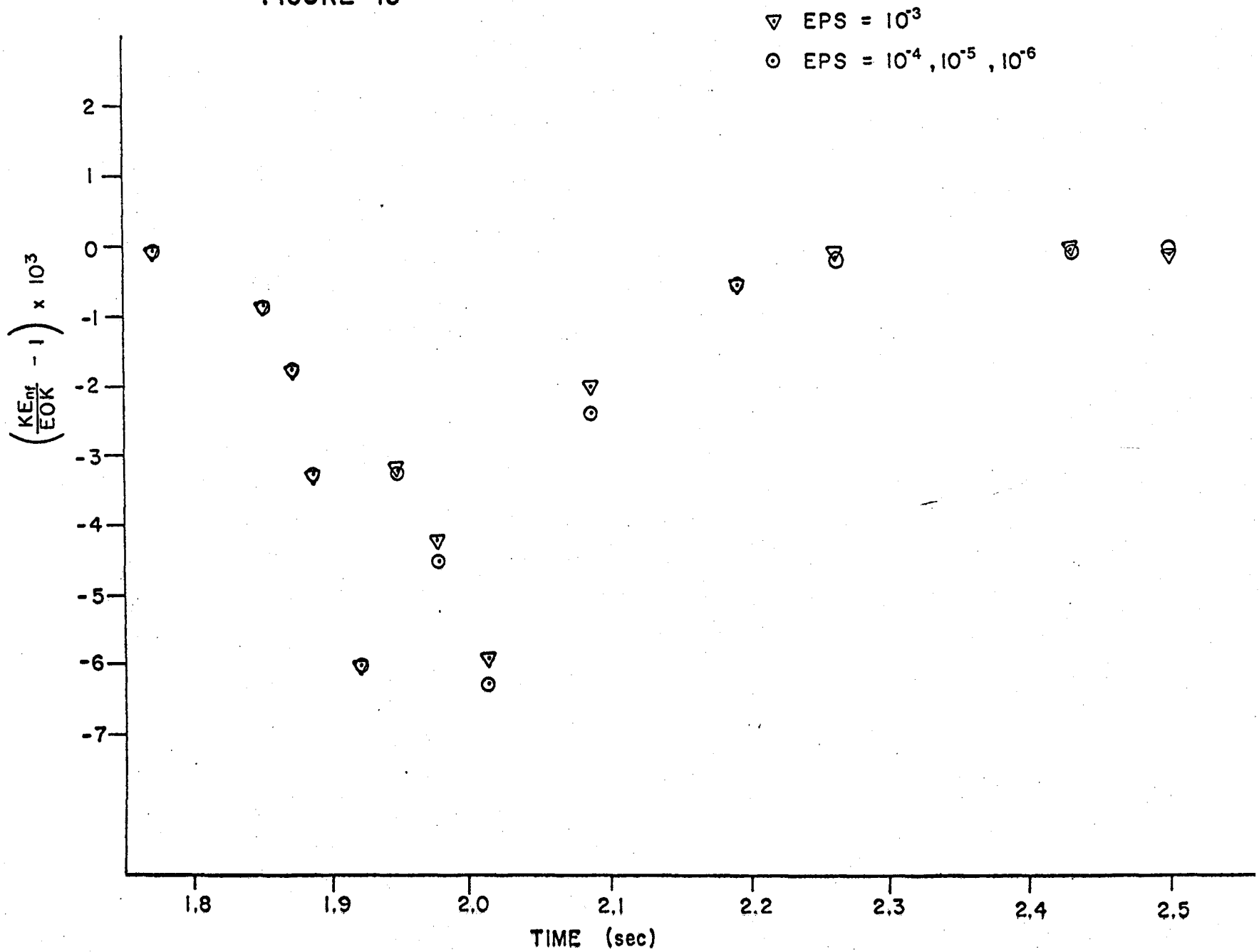
▽ EPS = 10^{-3}
⊙ EPS = 10^{-4}, 10^{-5}, 10^{-6}
$\left(\frac{KE_{nf}}{EOK} - 1\right) \times 10^3$
2
1
0
-1
-2
-3
-4
-5
-6
-7
1.8
1.9
2.0
2.1
2.2
2.3
2.4
2.5
TIME (sec)

FIGURE 14 NORMALIZED FLUX vs POSITION

T = 2.01 sec
NORMALIZATION FACTOR = $\frac{1}{3187}$

• eps = 10^{-6}
+ eps = 10^{-5}
o eps = 10^{-4}
▽ eps = 10^{-3}
} SAME

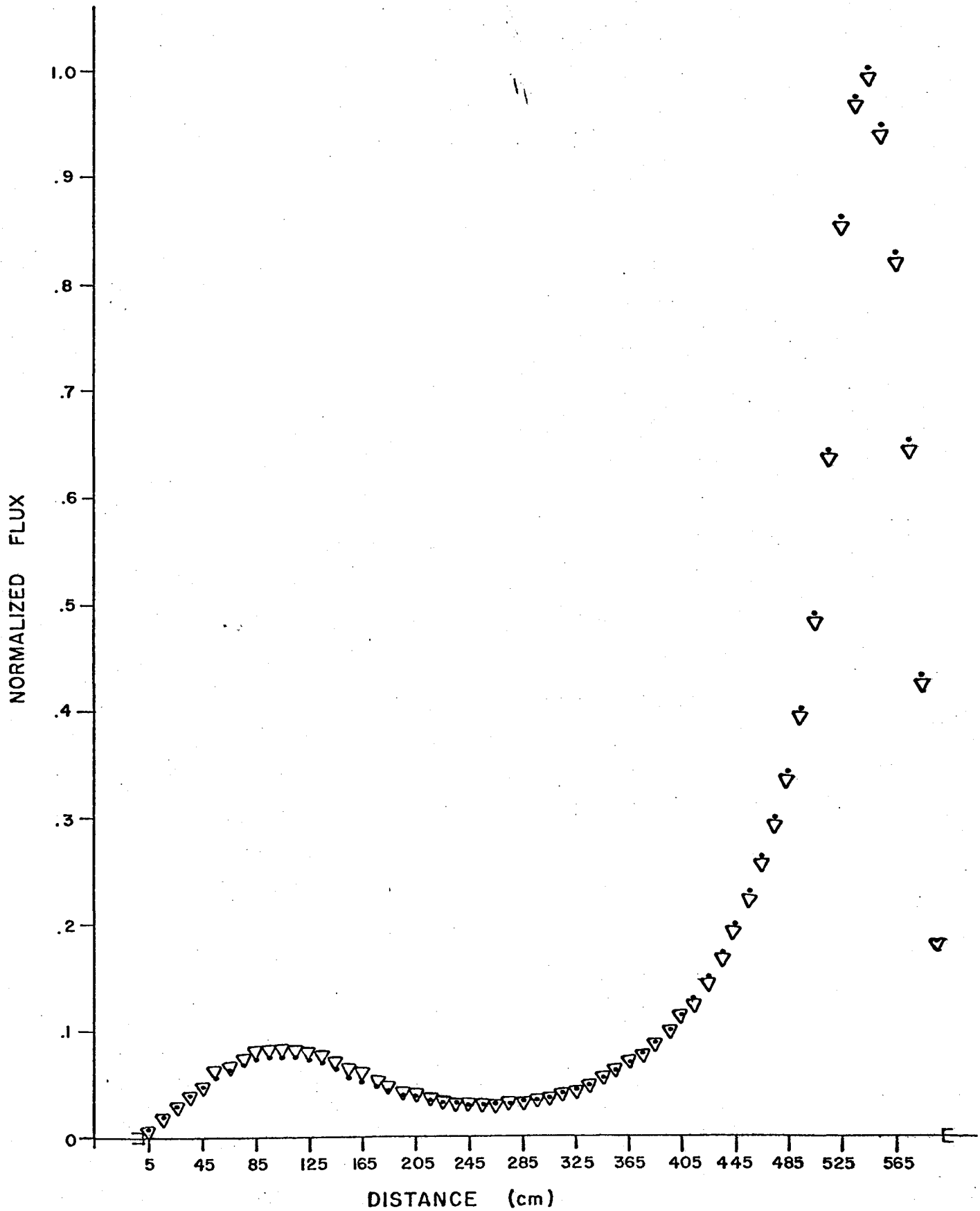

FIGURE 15 NORMALIZED FLUX vs POSITION

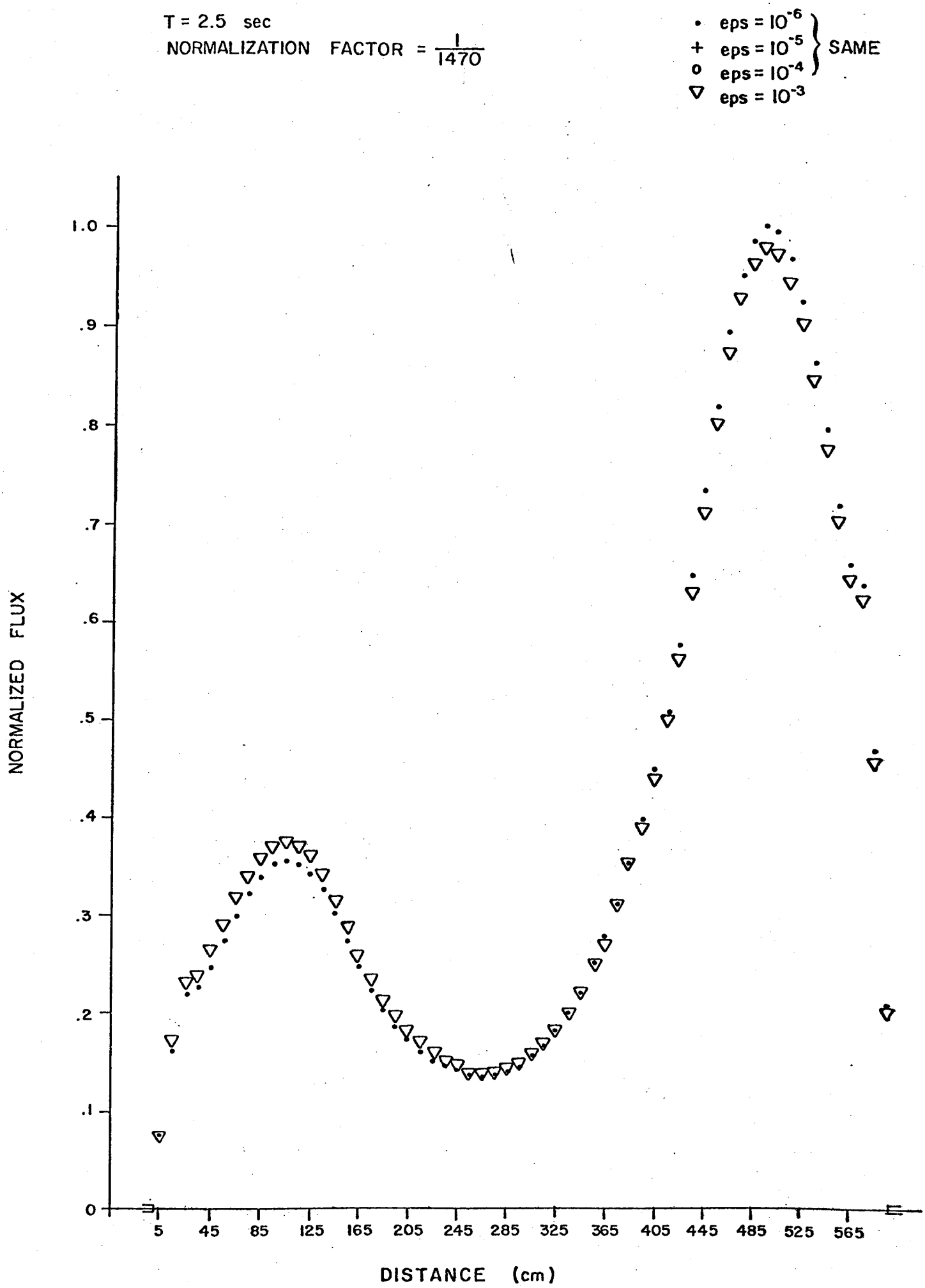

APPENDIX

The matrix equation:

$$\bar{A}\ \bar{X} = \bar{Y}$$

where $\bar{Y}$ and $\bar{A}$ are n x n, and $\bar{X}$ is 1 x n, may be solved by assuming an iteration of the form:

$$\bar{X}^{p+1} = -(\bar{L}+\bar{D})^{-1}\bar{U}\bar{X}^{p} + (\bar{L}+\bar{D})^{-1}Y \qquad 1$$

where p is the number of the iteration, and $\bar{L}$, $\bar{D}$ and $\bar{U}$ are lower triangular, diagonal, and upper triangular respectively such that:

$$\bar{A} = \bar{L} + \bar{D} + \bar{U} \qquad 2$$

It can be easily seen from Equation 1 that if at some state $\bar{X}^{p} = \bar{A}^{-1}\ \bar{Y}$, then $\bar{X}^{p+1} = \bar{A}^{-1}\ \bar{Y}$. It can be shown[9] that if a_{ij} is the ij'th element of A and if:

$$|a_{ii}| \geq \sum_{j} |a_{ij}| \ , \ (j \neq i)$$

with inequality for some i, then the proposed iteration method converges. Equation 1 is called the method of successive displacement, or Gauss-Seidel method.

Equation 1 can be written:

$$\bar{X}^{p+1} = \bar{X}^{p} + \bar{r}^{p} \qquad 3$$

with:

$$\bar{r}^p = - (\bar{L}+\bar{D})^{-1}(\bar{A}\bar{X}^p-\bar{Y}) \qquad 4$$

We can anticipate further corrections to $\bar{X}^p$ by overcorrecting (or perhaps undercorrecting) in the hope of speeding the convergence of the iteration. The iteration may then be written:

$$\bar{X}^{p+1} = \bar{X}^p + \alpha\ \bar{r}^p \qquad 5$$

where α is a real number called the Liebmann acceleration parameter. For $\alpha > 1$, we speak of over-relaxation. For $\alpha < 1$, we speak of under-relaxation. Again, if $\bar{X}^p = \bar{A}^{-1}\ \bar{Y}$, then the iteration yields $\bar{X}^{p+1} = \bar{A}^{-1}\ \bar{Y}$, proving consistency. It can be shown[9] that proper choice of the Liebmann acceleration parameter can sometimes increase the convergence rate by an order of magnitude.

REFERENCES

(1) A.F. Henry, "Nuclear Reactor Analysis", MIT Press, Cambridge, Massachusetts (1975).

(2) G. Kugler, TDAI-95, (1975).

(3) V.K. Mohindra, and A.R. Dastur, American Nuclear Society Transactions, Toronto (June, 1976).

(4) A.R. Dastur and D.B. Buss, AECL-5181 (1975).

(5) W.M. Stacey, Jr., "Space-Time Nuclear Reactor Kinetics", Academic Press, New York (1969).

(6) D.A. Meneley, K.O. Ott and E.S. Wiener, Trans Am Nuclear Society, II, 225 (1968).

(7) P.M. Garvey, RSDWP-N-6, Unpublished, AECL Report (1975).

(8) K.O. Ott and D.A. Meneley, Nuclear Science and Engineering, 36, 402-411 (1969).

(9) M. Clark, Jr., K.F. Hansen, "Numerical Methods of Reactor Analysis", Academic Press, New York (1964).